Final Report

STUDY OF PLASMA ENVIRONMENTS FOR THE INTEGRATED SPACE STATION ELECTROMAGNETIC ANALYSIS SYSTEM

NASA/MSFC, Contract # NAS8-36955

(July 27,1991 through August 26,1992)

IN-18-CR
P. 64

Principal Investigator : Nagendra Singh

Department of Electrical and Computer Engineering
University of Alabama
Huntsville, AL 35899

(NASA-CR-192513 STUDY OF PLASMA ENVIRONMENTS FOR THE INTEGRATED SPACE STATION ELECTROMAGNETIC ANALYSIS SYSTEM Final Report, 27 Jul. 1991 - 26 Aug. 1992 (Alabama Univ.) 64 p

N93-13152

Unclas

G3/18 0131693

CONTENTS

SUMMARY :

Effect of arc due to the negative grounding of the structure of the Space Station *Freedom* (SSF) are analyzed. A circuit model is constructed to evaluate the transient effects on the solar cell array and the load on the power system. The results from the transient analysis show that the load power is minimally disturbed; However, the perturbations critically depend on the capacitances of the solar cells to the plasma and another capacitances in the system. If such capacitances are relatively large (> 200pF per cell) the perturbation in the negative parts of the array, and hence in its power generation capability, are likely to be significant. The transient effects are analysed using lumped and distributed circuit parameters. The latter model predicts a significant effect on the solar cells near the negative end of the array.

The electrostatic, magnetostatic and radiation fields generated by arcing events are analyzed. The fields critically depend on whether the electrons ejected during the arcing are escaping along the earth's magnetic field or they are returned to the spacecraft. The generation of electrostatic fields for the former case is calculated by assuming that the ejected electrons set up an electron beam along the earth's magnetic filed. Estimate show an electrostatic field of the order of about 7V/m, and the magnetostatic field about ten times the earth's magnetic field at the SSF altitudes. These estimates are based on the arc currents measured in the laboratory tests at NASA/MSFC.

The generation of radiation fields are examined for both the possibilities dealing with the escape and return of the ejected electrons. In the former case of escaping electrons, the radiation occurs from a relatively long monopole. An estimate of the radiated power into the ionospheric plasma indicates that the radiation is so large that it can critically affect the arcing process and it can limit the arc current. The radiation loss dictates that the arc current be limited to about ~200 A. In a laboratory experiment, the radiation process are

not likely to occur because of the size of the plasma device. Therefore, this limiting process may not be operative in laboratory measurements and large arc currents can be measured. The radiation fields generated by the escaping electrons are estimated, and they are found to significantly the SSF electromagnetic environments, in the frequency range from a few kHz to about 1 MHz.

If the electrons do not escape along the magnetic field, the radiation is likely to occur from a small volume near the arcing spot. This is modeled as a radiation loss from a short monopole. Such small structures predominately radiate electron plasma waves. The estimate of the radiated power into plasma waves indicates that when such waves are Landau damped, the ambient plasma around the station will be significantly heated; plasma temperatures up to 100 eV is expected. It appears that if the arcing is frequent and randomly distributed over the entire surface of the station, a hot plasma will eventually engulf the Space Station Freedom.

It is recommended that the local dynamics of electrons, including charge neutralization process be clearly understood for the purpose of establishing the electromagnetic effects on a firm theoretical foundation.

When the control of the charge on the SSF structure is exercised by a plasma contactor, the major concern is about the stability of such a device . If the interruption in the current ejection from the contactor by plasma instability is severe, the structure may charge to the arcing potentials. The stability of plasma contactors remains unexplored. Before a plasma contactor is totally relied upon, it is urgent that the stability issue is examined thoroughly.

Measurements during the flights of the space shuttle have shown that the environment of a large spacecraft in space is contaminated by a broadband electrostatic noise in the frequency range from zero to a few tens of khz. The source of the noise is identified to be ions produced by the exchange of charge from the dominant O^+ ions to the contaminant molecules, which

are found to be predominantly H_2O [e.g., see Cairns and Curnett , 1990]. It is believed that the noise is generated by an instability driven by a beam of water ions moving perpendicular to the geomagnetic field lines. Measurements normally give fields in the saturation state of the instability. We have shown here that during the growth phase of the instability after a release of water vapour, intense fields upto 50 V/m, depending on the water ion density are likely to be generated near the lower hybrid frequency ($\sim$ 5kHz). This is in contrast to the measured field levels $<$ 100 mV/m in the saturation state. However, measurements seem to underestimate the fields due to the measuring antenna size [Cairns and Gutnett, 1990]. The theoritically established fields in the saturation state are found to be higher than the measured fields by an order of magnitude. It is recommonded that the discreparency between the measurements and the heuristically derived theoritical results be reconciled by further data analysis and regorous theoritical calculations. This will allow a better definitation of the electromagnetic environment of the Space Station Freedom.

The motional EMF drives a current in the spacecraft structure. The wave generated by such currents are also analysed and heuristically the amplitude levels of electric and magnetic fields and their frequency range are estimated. A summary of our effort reported here can be found in diagram (I).

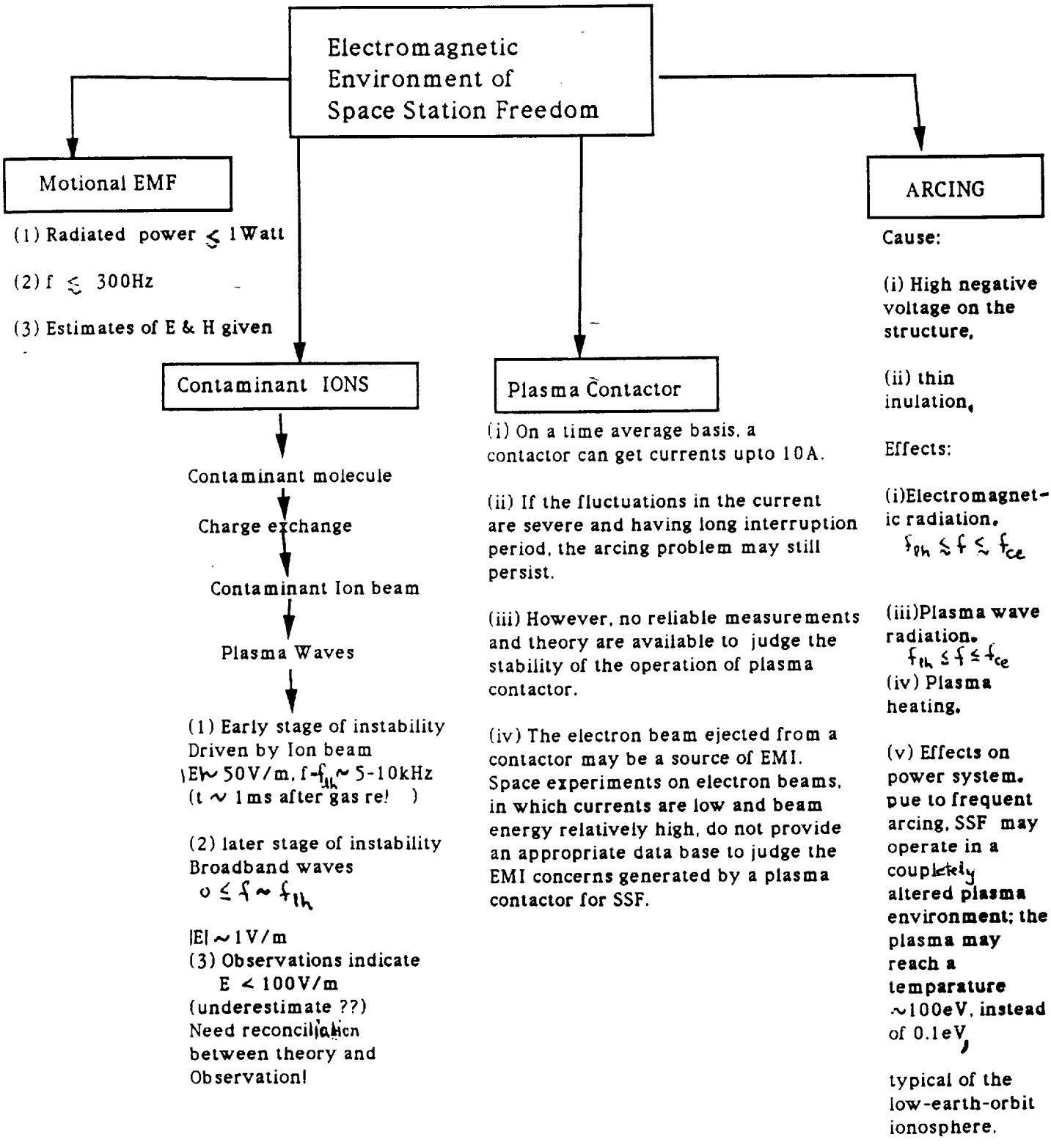

Diagram I A brief summary of the report.

1 Introduction

The relatively high power requirement of the Space Station *Freedom* (SSF) has led to the power system design operating at a relatively high voltage of 160 volts. The power will be generated by solar-cell arrays. When solar cell arrays float in the ionospheric plasma, a major part of the array ($\leq$ 90%) attains a negative potential with respect to the plasma, while only a small portion ($\leq$ 10%) attains positive potentials. This is primarily determined by the relatively large mobility of the electrons with respect to the O^+ ions in the ionosphere.

The design of the various components of the power systems has also led to the necessity of grounding the SSF structure to the negative end of the solar arrays. Figure 1 schematically illustrates this grounding scheme: N solar cells are connected in series to produce the required voltage of 160 V and the required current is produced by connecting M strings in parallel. When the total voltage generation V_o is 160 volt, the negative end of the arrays and the SSF structure attain a potential of about -140 volt with respect to the ambient plasma. In addition to this relatively large negative potential on the structure, another complicating factor is that the entire structure is insulated by a 3 μm thick coating of Al_2O_3. This insulation layer is likely to float at about -1 volt with respect to the ionospheric plasma. This is a consequence of an ion- rich sheath formation around a floating body. This leads to a potential drop of about -139 volt across the thin insulating layer. The electric field in this layer attains a value given by

$$\mathrm{E} = (139/3) \times 10^6 = 5 \times 10^7 V/M$$

Such large fields inside the insulating layer are likely to cause dielectric breakdown and arcing.

Recent laboratory tests on negatively biased specimens of the material to be used for the SSF structures in a plasma chamber at NASA/MSFC show strong arcing events, whish

create about 1 mm diameter craters all over the specimen surface [R. Curruth, private communication, 1991]. Arc currents up to 1500 A have been measured.

The purpose of this report is to present results of our investigations on electromagnetic effects of such arcing. The investigations include studies on (1) transient effects on the power system due to discharging and charging of the structure and (2) electromagnetic field generation and radiation from the arc.

In addition to the arcing and its effect, we also discuss (1) concerns regarding the stability of the operation of a plasma contactor and the asss EMI concerns arising from it, (2) electric and magnetic fields generated by contaminant ions and (3) electromagnetic fields caused by the current flow in the structure due to the motional EMF.

2 Transient Effects on the Power System Due to Arcing

A large arc current is likely to induce transients in the power system. For the power system safety, it is important to asses the magnitudes of the transients induced in various components of the system. In order to estimate the amplitude, we use lumped and distributed circuit models for the system components such as solar-cell array, the load and the structure and their interconnections, and the interaction with the plasma. The lumped circuit model is shown in Figure 2. The distributed circuit model is discussed later in section 3. We will shortly discuss various lumped elements included in the circuit. It is important to point out that for arcs with rise time $t_r > 1$ms, the frequency spectrum of interest in this problem is ≤ 10 khz. For such frequencies, the free space wavelength $\lambda \geq 30$ km. For the SSF, the dimensions of the various structures are limited to $\leq$100 m. Thus the lumped-circuit description appears to be satisfactory. However, a variety of wave modes and wavelengths occurs in a magnetoplasma compared to that in free space. Therefore, extreme caution must be exercised in utilizing the predictions from a lumped circuit model.

The various elements in the lumped-circuit model of Figure 2 are described here. The solar cell array is represented by a voltage source V_A, the series resistance R_A and parallel capacitance C_A. R_L is the total load on the array. The parallel RC circuits consisting of C_I and R_I and C_E and R_E represent the ion and electron collection by the negative and positive portions of the array, respectively. The loop consisting of C_D and R_D represents the discharge circuit; this parallel combination determines the magnitude of the arc current and its temporal evolution. The rest of the resistance R_S, R_R, and R, whcich are negligibly small, are simply introduced to monitor the current flows at desired locations in the circuit.

For determining the values of the capacitances and resistances, we have followed Metz [1986]. In order to meet the power generation requirements, a solar cell array consists of a

parallel combination of several solar cell strings (Figure 1) which consist of a series connection of desired number of solar cells. If the operating voltage is V_A and each cell generates δV_A volts, the number cells in a string is

$$N = V_A/\delta V_A \tag{1}$$

Furthermore, if the generated power is P watts, the required current in a matched load I=P/V_A. If the opening current of a cell is δI, the number of strings in parallel is

$$M = P/(\delta I V_A) \tag{2}$$

Assuming P to be 80KW and δI$\sim$ 1A, M = 500, if δI is only 100mA , 5,000 strings are needed.

If the conductivities of the sheaths near the positive and negative cells are α_e and α_i, respectively, the sheath resistances R_E and R_I are given by

$$R_E^{-1} = (1-\delta)NM\alpha_e \tag{3}$$

$$R_I^{-1} = \delta NM\alpha_i \tag{4}$$

where δ is the fraction of the array at negative potentials [Metz, 1986]. Typically $\delta \simeq 0.92$, $\alpha_e \simeq \times 10^{-6}$, and $\alpha_i \simeq 2 \times 10^{-8}$ [Metz,1986], giving $R_E \simeq 65\ \Omega$ and R_I= 679 Ω. The sheath capacitance C_E and C_I are difficult to estimate. However, if the average capacitance of each cell to the plasma is C_P

$$C_E \approx (1-\delta)NMC_P \tag{5}$$

$$C_I \simeq \delta NMC_P \tag{6}$$

The value of C_P ranges anywhere from 2 to 200 pf [Metz, 1986]. In order to achieve an understanding of how this capacitance alters the transient behavior, we presented calculations for C_P = 2pf, 200pf and 2,000 pf. However, the major part of the following discussion is based on C_P = 200pf, for which

$$C_E = 1.3 \times 10^{-6} F \text{ and } C_I = 1.6 \times 10^{-5} F$$

The parameters of the discharge are the capacitance (C_D) between the plasma and the structure, and the dynamic resistance (R_D) of the arc itself. Calculation is carried out for a value of C_D determined by treating the structure-plasma as a parallel plate capacitor. The dynamic resistance is modeled to approximately yield the temporal evolution of the arc current measure at NASA/MSFC [R.Curruth, Private Communication,1991].

A typical example of measured arc current is shown in Figure 3a. It has a fast rise time of about ≤ 0.1 ms and then decays relatively slowly. The peak current is about 1500 A. The frequency spectrum of the current is shown in Figure 3b. It is seen that there is an appreciable current even at large frequency of about 12 kHz. For such relatively low frequencies, inductive impudences are estimated to be negligibly small.

In the analysis presented below, the structure capacitance C_D is assumed to be $10^3 \mu$F. This is roughly the capacitance of a metallic surface of area $\sim 300\ m^2$ coated with a 3 μm thick layer of Al_2O_3. The steady rate voltage drop across this capacitance (see Fig. 2) is

$$V_{CD} = V_A \frac{R_I}{R_I + R_E} \approx 146V \tag{7}$$

Discharge: In order to simulate the arcing which discharges the structure capacitance, the dynamic resistance is suddenly reduced and it is varied with time so that the discharge current I_D closely approximates the measured arc current (Figure 3a). Figure 4a shows the simulated time history of the dynamic resistance R_D. Figure 4b shows the arc current flowing through the discharge circuit. It reaches a maximum amplitude of about 1500 A. The temporal evolution of the discharge capacitor is shown in Figure 5. the capacitor almost completely discharges as indicated by the minimum voltage of about ~ 1 volt.

In response to the discharge, a current injected into the circuit at node "4". This current is measured by putting a small resistance R_R as shown in Figure 2. In response to this current

injection, the currents and voltages in the main part of the circuit, which consists of the load and the solar cells, are affected. The temporal evolution of the injected current is shown in Figure 6. It is interesting to note that even though the maximum arc current is 1500 A, the maximum current injected into the power system is only about 23 A. However, this current critically depends on the impedence between the nodes 'O' and '4' in the circuit Figure 2. This impudence is a parallel combination of C_I, R_I and the impudence involving R_L, R_A, C_A and the parallel combination of R_E and C_E. When C_I becomes large, it tends to short circuit all other impedances and a large injected current results. For example, when C_I is increased to 1.5×10^{-4}F, the injected current increases to 240A, and most of the injected current flows through the capacitance C_I. However, a word of caution must be added here. In the circuit model used here, the entire capacitance of the negative part of the array is lumped to node '4', the extreme negative end of the array. In reality this capacitance is distributed over the negative part of the array. Therefore, the injected current is likely to flow through some part of the array before it is shunted to the ground. If the injected current is large, it may damage the solar cells. For example, when $C_I = 1.5 \times 10^{-4}$F, the injected current of 240 A is a significant fraction of steady -state array current of 500 A. Such an injected current can significantly alter the operating conditions of the solar cells near the extreme negative end of the array. On the other hand when C_I is reduced to 1.5×10^{-6}F, the injected current is only 2 A. Therefore, is is important that the capacitances of the solar cells to the plasma be properly estimated. This task require a knowledge of the geometrical features of the cells and the plasma sheath. The effects of distributing C_I over the entire negative end of the array is discussed in section 3.

Figure 7 shows that in response to the arc, the current through R_A, suddenly increases from 498.6 to 500.7 A. However, rigorously speaking this response is expected to have a greater perturbation in the current as discussed above, and later in section 3.

The perturbation caused in the load is shown in Figures 8a, 8b and 8c, which give the temporal evolution of the load current, voltage and power, respectively. The maximum perturbation in the load current is 1A, and the corresponding perturbation in the load power is about 200 watt, or about 0.3%. Thus, from the analysis presented here, it appears that arcing may not significantly affect the power system. However, this is more so if the array capacitance to the plasma is sufficiently small ($\leq$ 200 pf/cell).

Recharging: It is interesting to examine how the system perturbed by the arcing recuperates and the steady-state condition is re-established. Figure 5 shows that after the arcing event, it takes about 200 ms for the structure capacitance to charge 96% of the steady-state voltage drop.

Figures 9a and 9b show the collection of electron current I_E (through the resistor R_E in Figure 2) and ion current I_I (through the resistor R_I in Figure 2), respectively. It is seen that in response to the arcing, (see Figure 9a) I_E increases from the steady- state value of 0.21 A to 2.26 A, and I_I decreases (Figure 9b) from the same steady-state value to a negligibly small current of $<$ 0.005 A. The significant changes in the values of I_E and I_I suggest that the arcing has substantially changed the operating condition of the array; a larger portion of the array acquires positive potentials with respect to the ionosphere and a negligibly small portion remains negative with respect to the ionosphere. therefore, for the sake of rigor it is desirable that the circuit elements C_E, R_E, C_I, and R_I should vary with time during the transient phase. However, this has not been done here .The increased electron current is responsible for recharging the structure capacitance and it takes about 200 ms to achieve the recharging (Figure 5). As the recharging process continues, I_E and I_I relax to their steady-state values as shown in Figures 9a and 9b, respectively.

The main conclusion to be drawn from the analysis presented here is that the arcing is not likely to be disruptive so far as the load is concerned, if the capacitance between the

solar cells and the plasma is sufficiently small. When arcing occurs, a portion of the array initially at relatively large negative potentials is likely to carry a relatively large current if the solar cell capacitance C_P is sufficiently large. Such large currents may drastically change the operating conditions of the solar cells and hence their power generation capabilities. This may affect the power generation. However, the conclusion drawn here are only tentative so far because the details of the power system are not included in the analysis. It is desirable that the layout of the solar cells and the details of their interconnections be made available so that an exact analysis can be performed. The results presented in this report are based on an illustrative example.

3 Distributed circuit model.

The next step of analysis is done by distributing the solar cell capacitance all over the array. This model is constructed by grouping a certain numbrer of solar cells together; the equivalent circuit for the groups consisting of the negative and positive portions of the array are shown in Figures (10) and (11) respectively. The equivalent circuit of each group has a voltage source, a source resistance, a parallel capacitance and the resistance and capacitance to the plasma. The complete distributed model is shown in Figure (12), in which equivalent circuits of the groups of solar cells are connected to gether.The various elements in each group are described here. The negative portion is represented by a series resistance (RA1) and parallel capacitance (CA1). The couplling between the negative portion and the plasma through a sheath is represented by a parallel RC circuit consistlng of C_I and R_I as shown in Figure (10). The group voltage is represented by voltage source V11. The positive portion of the array is represented by a series resistance (RA2) and parallel capacitance (CA2). The coupling between the positive portion and the plasma sheath is represented by a parallel RC circuit consisting of C_E and R_E as shown in Figure (11). V12 represents the group voltage.

For an example, we used 5 solar cells in each group. Therefore, 32 groups are connected in series to produce the required voltage of 160 volt. There are M strings conected in parallel to produce the required current. The different components of each group are calculated as follows. The series resistances (RA1 & RA2) are given by:

$$RA1 = RA2 = RA \quad (total\ array\ resistance)/number\ of\ groups \tag{8}$$

The parallel capacitances (CA1 & CA2) are given by:

$$CA1 = CA2 = CA \quad (total\ array\ capacitance)/number\ of\ groups \tag{9}$$

The sheath resistance R_E and R_I are given by equations (3) and (4) with N = 5 and

M=5000. The sheath capacitances C_E and C_I are given by equations (5) and (6) with N= 5, M = 5000. For the discharge circuit we used the same model as in the lumped circuit model. Also, the load is represented by a resistance (RL).

Simulation is performed with different values of (C_P), but results are obtained for which C_P = 200pF, C_E =4 $\times$ 10^{-7}F, C_I = 4.6 $\times$ 10^{-6}F. Figure (13) shows that the perturbation in the array current decreases as we move from the negative end toward the positive end of the array. This happens due to the fact that the injected current at the negative end of the array flows toward the load and the positive end. In its way, an amount of current leaks out to the sheath through the impedences between the array and the plasma sheath. It is worth noting thatt the perturbation in the array current near the negative end is significant.

4 Quasi-static Electric and Magnetic Fields Produced by the Arc.

In an arcing event, electrons are injected into the ionospheric plasma. These electrons create a negative space charge and hence electric fields. Furthermore, the current itself also creates a magnetic field. It is important to know the magnitude of such fields generated in the vicinity of the SSF. The fields calculated here are not the radiation fields, which will be discussed in Section 4.

The magnitude of the electric field created by the space charge critically depends on the dynamics of the ejected electrons during the arcing event. The ejected electrons are restricted to move along the local earth's magnetic field as shown in Figure 14. when electrons are ejected, the negative charge on the metallic surface is diminished, leaving the positive charge near the insulating surface bare. A major issue here is how the positive charge is neutralized. Is it neutralized by areturn electron current distributed over a large volume, as indicated in Figure 14, or by returning the ejected electrons locally? In reality, it will be a mixture of both these processes. However, the ejected electrons are restricted by the magnetic field and, therefore, the neutralization of the bared positive charge far from the arc location must involve return current from a large volume. This issue is yet nor fully resolved. Therefore, we perform our calculations here on the basis that some of the ejected electrons do escape and corresponding ejected current, I_{ej}, is a fraction of the arc current I_{arc}. However, the fraction is not known.

As mentioned earlier, the electrons injected into the plasma are primarily guided along the earth's magnetic field lines. a typical electron is likely to undergo a helical motion as shown in figure 14. This motion produces an electron beam with a radius (r_b) equal to the

average Larmor radius of the ejected electrons. This radius is given by

$$r_b = r_L = (U_b sin\theta + V_{te})/\Omega_e \tag{10}$$

where U_b is the velocity of an ejected electron, θ is the pitch angle with respect to the magnetic field, V_{te} is the random thermal velocity of the electrons, and Ω_e is the electron cyclotron frequency.

The ejected current (I_{ej}) flows in a channel of radius r_b giving a current density

$$J_b = I_{ej}/\pi r_b^2 \tag{11}$$

This current is carried by electrons moving along the earth's magnetic field with a velocity $V_b cos\theta$. The negative space charge density in the beam can be approximated by

$$\rho_b = -en_b \simeq -I_{ej}/(\pi r_b^2 U_b cos\theta) \tag{12}$$

Assuming that this charge is neutralized by ions at a radius r$\simeq$ r_b, the boundary of the channel, the maximum electric field is estimated to be

$$E_{max} \simeq \frac{1}{2\pi\epsilon_0}\frac{1}{r_b}(\pi r_b^2)\rho_b \tag{13}$$

This field is calculated by assuming that the space charge is uniformly distributed, in a long cylinder of radius r_b along the earth's magnetic field. Substituting for ρ_b from (2), we obtain

$$E_{max} \simeq \frac{I_{ej}}{2\pi\epsilon_0}\frac{\Omega_e}{(U_b sin\theta + V_{te})U_b cos\theta} \tag{14}$$

For pitch angle near $\theta = 90^0$, the above expression is not valid because ejected electrons stagnate their the arc location and an electron beam is not likely to form. It is important to note that I_{ej} may or may not be the same as the arc current.

In order to get a numerical estimate for the fields, we assume B_o = 0. 3 Gauss, arcing voltage ϕ_o = 120 V and the ejected current to be the same as the arc current I = 1500 A.

Using these parameters, we obtain

$U_b \simeq \sqrt{2e\phi_o/m_e}$ = 6571 km/s, $r_b = r_L = 1.2 \sin\theta$ m and $E_{max} \simeq 6.8$ V/m when $\theta = 45^o$.

The location of the maximum field is expected to move with the moving clumps of ejected electrons. During the duration of the peak current lasting over about 10^{-4}seconds, such fields can be present over a distance of about s$\simeq 10^{-4}s \times 6571 \times 10^3$km $\simeq$ 657m along the field line from the location of the arc.

The escaping electrons generate a magnetic field. Assuming the electron beam as a line current source, the magnetic field for r$\geq r_b$ (see Fig. 14) is given by

$$B = \mu_0 I_{ej}/2\pi r \tag{15}$$

where r is the radial distance from the center of the ejected electron beam . For $I_{ej} = I_{arc} \simeq$ 1500A, B = 3/r Gauss. thus, in the vicinity of the ejected electrons (r$\simeq$ 1m) the magnetic field generated by the arc current is about ten times the earth's magnetic field at the altitude of the Space Station Freedom.

5 Electromagnetic and Plasma Wave Radiation Due to Arcing

There are two major sources of electromagnetic and plasma wave radiations during an arcing event. One is the arc itself. It acts like a radiating element in a medium which is a magnetized plasma. the other source is the radiation from the transient currents set up in various parts of the power system due to the arc, as discussed earlier in Section 2. In order to estimate the radiation level from the latter source, a detailed analysis of the spatial distribution of the transient current in the power system including cables and power lines is needed. Since the analysis of the spatial distribution is not available, the calculations on the radiation level from this source is postponed. However, it must be mentioned that the large structure and the system size of SSF suggest that the transient current distributed over a large volume will act like a relatively large antenna and hence a potent source of electromagnetic radiation.

The radiation from the arc current itself can be studied by assuming that the arc current is a current filament radiating into the ionospheric plasma . Quite often while carrying out such an analysis, the plasma medium is ignored. We show here that for the transient behavior of an arc occurring on SSF, the neglect of the ionospheric plasma effects is incorrect. A literature survey of phenomenon of arcing in connection with SSF and solar cell arrays indicated that the rise time of an arc typically ranges from ~ 0.1 ms to $\sim 1\mu$s. such rise times correspond to a frequency spectrum ranging from 10 kHz to 1MHz. For this frequency band, plasma effects are maximized because this band is bounded by the lower-hybrid and the electron-cyclotron frequencies in the ionosphere. Only at frequencies f$\geq$ 10 MHz, the plasma effects on the electromagnetic radiation are like to be ignorable.

For the expected altitudes of SSF, the characteristic plasma frequencies are as follows. The typical value of the magnetic field in the ionosphere is about 0.3 Gauss, and the plasma density is expected to range between 10^{11} to $10^{12}m^{-3}$. The corresponding characteristic

frequencies are as follows.

$$electron - cyclotron frequency: \qquad f_{ce} = \frac{1}{2\pi}\frac{eB_o}{m_e} = 0.87MHz \tag{16}$$

$$O^{+} cyclotron frequency: \qquad f_{ci} = \frac{m_e}{M_i} f_{ce} = 30Hz \tag{17}$$

$$Lower - hybrid frequency: \qquad f_{lh} = \sqrt{f_{ce} f_{ci}} = 5kHz \tag{18}$$

$$Electron - plasma frequency: f_{pe} = \frac{1}{2\pi}\left(\frac{n_0 e^2}{m_e \epsilon_o}\right)^{1/2} \simeq 3 - 9MHz \tag{19}$$

$$Ion - plasma frequency: f_{pi} = (m_e/m_i)^{1/2} f_{pe} \tag{20}$$

In the expressions for frequencies appearing above B_o is the earth's magnetic field, M_i and m_e are the ion and electron masses, respectively, and n_0 is the plasma density. the plasma frequency ranges from 3 MHz to 9 MHz when n_0 ranges from $\sim 10^{11}$ to $10^{12} m^{-3}$.

The dielectric properties of the ionospheric plasma is determined by the signal frequency f and the characteristic frequencies given above. The ionospheric plasma is described by a dielectric tensor given by

$$\epsilon = \epsilon_o \begin{pmatrix} K_\perp & jK_H & 0 \\ -jK_H & K_\perp & 0 \\ 0 & 0 & K_{||} \end{pmatrix} \tag{21}$$

$$K_{||} = 1 - \sum_\alpha X_\alpha / U_\alpha \tag{22}$$

$$K_\perp = 1 - \sum_\alpha X_\alpha U_\alpha / (U_\alpha^2 - Y^2) \tag{23}$$

$$K_H = -\sum X_\alpha Y_\alpha / (U_\alpha^2 - Y_\alpha^2) \tag{24}$$

$$X_\alpha = f_{p\alpha}^2 / f^2, \qquad Y_\alpha = f_{ce}/f \quad and \quad U = 1 - j\nu_\alpha/\omega \tag{25}$$

and ν_α is the effective collision frequency.

In writing above expression for ϵ, is is assumed that the earth's field is along the Z axis. The summation in the above expressions are over the various charged-particle species in the ionosphere. However, for frequencies f$\gg f_{lh}$, ion dynamics can be ignored. For the arc with

rise time < 0.1 ms, this is approximately valid if one is interested in radiation during the early stage of the arc. For such high frequencies $\nu \ll$f, and the collision effects can be ignored.

When the signal frequency falls in the band f_{lh}<f$\leq f_{ce}$, the radiation from a source is confined within a cone with its axis along the magnetic field, and the apex on the source, as shown in Figure 15 [Singh and Gould, 1971]. The half-cone angle is given by

$$tan^2\theta_c = -K_\perp / K_{||} \tag{26}$$

For the frequency range of concern here $K_\perp$>0 and $K_{||}$<0, making $\tan^2\theta_c$ a positive number, and θ_c a real angle. If the frequency f$\ll f_{ce}$, the above expression for the half- cone angle is considerably simplified to

$$\theta_c \simeq tan^{-1}(f/f_{ce}) \tag{27}$$

For an arc with a rise time $\leq$ 1ms, the frequency of interest if f$\simeq$ 10 kHz. The half-cone angle for this case is given by

$$\theta \simeq tan^{-1}(10 \times 10^3/.84 \times 10^6) \simeq 0.67^0 \tag{28}$$

Thus the arc under consideration will radiate a highly collimated beam of electromagnetic and plasma waves, with half-beam width of about 0.67^0. This beam points along the earth's magnetic field. As the arc rise time decreases, the radiation frequency increases, yielding increasing half-cone angle and radiation beam width.

The major question to be answered now is about the amount of power radiation and the associated field strengths. This is difficult problem because radiation from sources in a magnetoplasma is not a well studied area.

In order to estimate the amount of radiated power, we use the theoretical formulation of Balmain [1964] and Singh and Gould [1971] for the radiation from a short dipole in a

magnetoplasma. An arc is modeled as a current filament over a ground plane as shown in Figure 15. The radiation resistance of the filament in full space s given by [Balmain,1964],

$$R_r = R_e(Z_{in}) \tag{29}$$

where

$$Z_{in} = \frac{a}{j\omega^2\pi\epsilon_o K_\perp L F^{\frac{1}{2}}}[ln(L/p) - 1 - ln(\frac{a + F^{1/2}}{2F})] \tag{30}$$

$$F = sin^2\theta + a^2 cos^2\theta \tag{31}$$

$$a^2 = K_\perp / K_{||} \tag{32}$$

θ is the orientation of the current filament with respect to the ambient field, L is the length of the current filament, and ρ is its radius. For the case of an arc, the current carrying electrons are guided along the field line and it is reasonable to assume that $\theta = 0$ for which Eq. (29) is simplified. for the monopole model of the radiation for the arc, the radiation resistance is given by

$$R_r = \frac{1}{4}\sqrt{\mu_o/\epsilon_o}\frac{1}{K_\perp}(\frac{\lambda_o}{2\pi L}) \simeq 30\pi\frac{1}{K_\perp}(\frac{\lambda_o}{2\pi L}) \tag{33}$$

Where λ is the free space wavelength at a frequency f.

The above expression shows that the radiation resistance $R_r \alpha L^{-1}$, implying that as L $\rightarrow$ 0, $R_r \rightarrow \infty$. This suggests an infinitely large radiation of power, and it is unphysical. Singh and Gould [1971] have shown that this unphysical result is the consequence of the assumption of the plasma being cold. If the warm plasma effects are included, the radiation resistance becomes finite when $L \rightarrow 0$. Therefore, Eq.(30) is valid when L$\gg 10\lambda_d$, where λ_d is the plasma Debye length. When L$\leq$ 10 λ_d, the radiation resistance is given by

$$R_r \simeq \frac{1}{8\pi}\frac{1}{K_\perp}\sqrt{\mu_o/\epsilon_o}(C/V_o)^3(\frac{2\pi L}{\lambda_o})^2 \tag{34}$$

where C is the velocity of light in free space, and V_o is the electron thermal velocity. The theory of Singh and Gould [1971] was developed for a uniaxial plasma, in which the magnetic field is so large that $f_{pe} \ll f_{ce}$. On the other hand, in the ionosphere, $f_{ce} \ll f_{pe}$. The factor $K_\perp^{-1}$ in (34) is included to account for this.

In order to have a feel for the radiation resistances, we assume that the ambient plasma density, $n_o = 4 \times 10^5 cm^{-3}$ for which $f_{pe} \simeq 6$MHz, $f_{ce} \simeq 0.84$ MHz and electron temperature $T_e = 0.2$eV, giving $C/V_o \simeq 1.6 \times 10^3$. With these parameters, the radiation resistance for 10 kHz is given by

$$R_r = 10^4/L \quad \Omega \qquad L \gg 10\lambda_d \tag{35}$$

$$R_r \leq 50L^2 \quad \Omega \qquad L \leq 10\lambda_d \tag{36}$$

where L is the arc length in meters.

If the arc length is known, the radiation from the arc can be estimated. If the current carrying electrons escape along the magnetic field lines, a good estimate for the current filament length is the distance travelled by the electrons having an energy of 120 eV over the rise time of the arc. This distance is of the order of kilometer. Since $\lambda_d \simeq 1$cm, equation (35) gives a radiation resistance of 10 Ω. Furthermore, if the entire arc current escapes, the power radiated is then calculated as

$$P_r \simeq \frac{1}{2} I_{arc}^2 R_r \simeq \frac{1}{2} \times (1500)^2 \times 10 \simeq 10^7 \quad Watt \tag{37}$$

The total energy radiated over the rise time is

$$W_{rad} \simeq P_r \triangle t \simeq 10^7 \times 10^{-4} = 10^3 J \quad !! \tag{38}$$

This is an enormously large energy.

The total energy discharged during the arcing is approximately given by

$$W_{discharge} \simeq \frac{1}{2}CV^2 \simeq \frac{1}{2} \times 10^{-3} \times (160)^2 \simeq 13 \quad J \tag{39}$$

A comparison of W_{rad} with $W_{discharge}$ clearly indicates that radiation losses are so severe that it is likely to quench the arcing process it self. It also suggest that the plasma around the space station will be strongly affected by the radiation. Working backward, it is possible to estimate the maximum bound (P_{max}) on the arc current:

$$\frac{1}{2}I_{max}^2 R_r \triangle t \simeq W_{discharge} \tag{40}$$

or

$$I_{max} \simeq (\frac{2W_{discharge}}{R_r \triangle t})^{1/2} \tag{41}$$

For the parameter used in the above discussion, $I_{max} \simeq 170$ A.

In laboratory, where the radiation process are not allowed by the size of the devices, current larger than I_{max} can be possible.

For such radiation-limited arc currents, the radiation fields in the cone of radiation (Fig. 15) can be estimated as follows. When $\theta_c \ll 90^0$, as is the case for f$\ll f_{ce}$, it can be assumed that the radiation is primarily electromagnetic and the radiation occurs in a medium with an effective dielectric constant given by

$$\epsilon_{eff} \simeq \epsilon_o(f_{pe}^2/f f_{ce}) \tag{42}$$

The corresponding effective medium wave impudence

$$\eta_{eff} = \sqrt{\frac{\mu_o}{\epsilon_{eff}}} \simeq 120\pi\sqrt{\frac{f f_{ce}}{f_{pe}^2}} \quad \Omega \tag{43}$$

The Pointing vector is given by

$$S_{av} = \frac{1}{2}|E|^2/\eta_{eff} \quad Watt/m^2 \tag{44}$$

where $|E|$ is the magnitude of the radiation electric field. Integrating S_{av} over the area of the radiation cone base (Fig. 15) at a distance r from the apex (Fig. 15), total radiated power

$$P_r \simeq \frac{1}{2}\frac{|E|^2}{\eta_{eff}}\pi r^2 tan^2\theta_c \tag{45}$$

Equating (43) with the radiated power determined by the radiation resistance R_r in (30), we obtain

$$|E| \approx \frac{I_{ej}}{\pi}\frac{\sqrt{R_r\eta_{eff}}}{r tan\theta_c} \quad V/m \tag{46}$$

When $f_{th} < f \ll f_{ce}$, the radiation fields are written as

$$|E| = 60\sqrt{\pi}\frac{I_{ej}}{r}\left(\frac{f_{ce}^2}{f f_{pe}}\right)\left(\frac{f f_{ce}}{f_{pe}^2}\right)^{\frac{1}{4}}\left(\frac{\lambda_o}{2\pi L}\right)^{\frac{1}{2}} \tag{47}$$

$$|B| = \mu_o|E|/\eta_{eff} = \frac{mu_o}{2\sqrt{\pi}}\frac{I_{ej}}{r}\left(\frac{f_{ce}^2}{f f_{pe}}\right)\left(\frac{f f_{ce}}{f_{pe}^2}\right)^{\frac{-1}{4}}\left(\frac{\lambda_o}{2\pi L}\right)^{\frac{1}{2}} \tag{48}$$

where B is the radiation magnetic field of the arc. Numerical estimates of the fields for f = 10 kHz, f_{pe} = 6 MHz and f_{ce} = 0.84 MHz arc given by

$$|E| \simeq 10^4\frac{I_{ej}}{\sqrt{L}}\frac{1}{r} \quad V/m \tag{49}$$

$$B \simeq 20\frac{I_{ej}}{\sqrt{L}}\frac{1}{r} \quad Gauss \tag{50}$$

It is worth mentioning that these fields are the far fields. In the close vicinity of the arc, the quasi-static fields given by equations (14) and (15) are valid. For a numerical estimate we assume r$\simeq$ 1 km, L $\simeq$ 100 m, and we find that

$$|E| \simeq I_{ej} \quad V/m \quad and \quad |B| = 2\times 10^{-3} I_{ej} \quad Gauss \tag{51}$$

Therefore if the injected current $I_{ej} = 100$ A, which is a fraction of the arc currents measured in laboratory, $|E| \simeq 100$ V/m and $|B| \simeq 0.2$ Gauss. These fields are a significant perturbations in the SSF electromagnetic environment.

Radiation of Plasma Waves: The above picture of the radiation holds good if the arc length is determined by the escaping electrons, carrying the arc current. If electrons do not escape, and they are confined into a small volume near the arc, the arc length $L \leq 10\lambda_d$, which is nearly the size of the sheath near the insulator. In this case, the radiation occurs in the form of electron plasma waves, and in that case equation (36) is the valid formula for the radiation resistance. for example, let us assume that $L \simeq 1$ cm and $I_{ej} = 1500$ A; the radiated power

$$P_r \simeq \frac{1}{2} I_{ej}^2 R_r \simeq 10 \quad kW \tag{52}$$

The energy radiated over the arc life time

$$W_r = 10 \times 10^3 \times 10^{-4} s \simeq 1 \quad J \tag{53}$$

This is about 8% of the total discharge given by equation (39).

The radiation of plasma waves suggest that the electrons in the close vicinity of the arc will be heated by Landau damping of the waves. Since electron plasma waves are likely to be intense near the arc, the ions will be also heated by non-linear plasma processes. The time scale for heating ions is f_{pi}^{-1} which is less than arc rise time. This ensures ion heating during the life of an arc. Simple estimates based on the radiated power, group velocity of the plasma waves, and the arc rise time suggest electron and ion temperatures in the excess of 100 eV.

If the arcing occurs often enough and randomly distributed over the entire surface area of the space station, the ambient ionospheric plasma will be highly modified. A plasma with a temperature of 100 eV engulfing the entire station is a distinct possibility.

6 Plasma Contactor

In previous sections, we discussed the effects of arcing due to the relatively large negative potential of the structure of the Space Station Freedom. It is now planned that the structure potential will be lowered by injecting electrons using a plasma contactor. Hollow-Cathode based plasma contactors have been developed for neutralizing the positive ions ejected from electric thruster systems [e.g. Ward and King, 1968], demonstrating that the electrons with currents of the order $\sim$ 1A can be ejected. However, in thruster applications the stability of the ejected current and EMI are probably not a major concern. In applications for the Space Station, it is not enough to eject electrons to lower the structure potential on a time average basis, but it is also of paramount concern to determine the impact of the operation of plasma contactor on the stability of the structure potential and the electromagnetic environment of the Space Station. A quantitative determination of the electric and magnetic fields generated by the currents and space charges associated with the aperation of the plasma contactor is a difficult task. Here our aim is only to highlight the major issues, which should be researched and resolved before a plasma contactor is fully trusted for the intended purpose of charge and potential control for the Space Station.

The central issue concerning the plasma contactor is the stability of the Space Station potential. This issue has hardly gotten any attention. Both laboratory [Wilber and Williams, 1990] and space experiments have been mainly concerned with the magnitude of the ejected curren, and likewise, modeling effects have been confined to steady-state analysis [Davis *et al.*,1988; Parks and Katz, 1987].

It is commonly believed that the electron dynamics in the electron ejection mode is resistive despite the fact that the plasma is essentially collisionless. The relatively large resistivity is attributed to plasma waves and turbulence driven by the ejected electron beam.

The questions, which naturally arise, are as fallow: Do the plasma wave, which provide the resistivity, modulate the ejected electron current ? What are the relative magnitudes and frequency spectrum of the modulation?

Answering these questions is essential because deep modulations with sufficiently long durations may inturrupt the electron ejection, and raise the potential on the structure of the spacecraft, and arcing may still occur. This defeats the whole purpose of operating the plasma contactor. Plasma waves, which are likely to be driven and have the potential of modulating current, may range in frequency from ion-cyclotron frequency to the electron-plasma frequency. The low-frequency modulations near ion- cyclotron frequency are potentially dangerous. In the close vicinity of the contactor, the dominant ion species will be that of the neutral gas emitted from the contactor. If the gas is Ar, the ion cyclotron frequency is about 10 Hz, which yields a modulation period of about 100 ms. If the current interrupts over such a time period, the charge accumulation on the structure can be increased by δQ$\simeq$-1C, if the steady-state current 10A is totally inturrepted over this period.Even if the current inturepts partially by 10%, $\delta Q \simeq$ -0.1C, which is sufficiently large to raise the structure potential above -100 V or so. Such charging and discharging may affect the stability of the entire power system.

The current modulations due to plasma instability has another consequence. The modulated electron beam in the volume near the contactor can be an effective radiator of plasma and elecromagnetic waves, which are potential source of EMI. Even crude estimates of the fields generated by this process are not available. Space experiments on electron beam ejections are not useful in this respect because the beam currents involved in them are relatively small limited to <100 mA and the beam energies are relatively high of the order of few eV [Neubert *et al.*, 1990; Kellogg *et al.* , 1986]. On the other hand, in the case of plasma contactor current can be as high as 10 A and the beam energy is limited to a few times the

ionization potential of the neutral gas used in the contactor. Thus, the beam energies are limited to a few tens of eV.

In view of the crucial role of the plasma contactor in ensuring safety of the Space Station structure and the stability of the power system, it is essential that the stability of the working of a plasma contactor in terms of its temporal variations be carefully researched. The study must be based on the both theory and modelling and as well as on laboratory measurements. the results from such studies must be reconciled so that a clear understanding of the stability is ensured.

7 Plasma Waves and Electric Fields Generated by Contaminated Ions

Space shuttle flights have amply demonstrated that the contaminants play an important role in determining the electromagnetic environment of a large spacecraft in the low earth orbit. In the case of the shuttle itself, water is the major contaminant. When water molecules undergo a charge-exchange with the oxygen ions, the major ion species in the ionosphere, a beam of H_2O^+ is created. such ion beams traverse perpendicular to the geomagnetic field lines and interact with the ionospheric plasma to generate plasma waves, which contribute to the electromagnetic environment of the spacecraft.

Space Station Freedom is a large spacecraft and its electromagnetic environment is likely to be affected by the contaminants. The purpose of this part of the report is to develop a predictive capability for the contributions of the contaminants to the electromagnetic environment of the Space Station, using measurements on waves and contaminants during the shuttle missions and appropriate linear and non-linear theories for plasma waves.

A detailed summary of the measurements on the contaminant molecules and ions, and waves during some space shuttle flights can be found in a technical report by W. S. Kurth, made to NASA Lewis Research Center [Grant NAG-3-449]. The report is a collection of papers in which measurements using the plasma diagnostic package (PDP) of the University of Iowa are reported and analyzed. Linear theories for the generation of plasma waves have been developed to explain the observations on the frequency spectrum of the waves [Cairns and Gurnett, 1991].

Our purpose here is not to dwell on the details of the instability which generates the waves, but it is an attempt to develop a working formula which can predict the electric field levels of the waves, and the frequency range over which the waves are likely to occur. In this connection we rely both on the measurements and the theory dealing with the saturation

of the wave. It is the saturated level of the waves which is normally measured. We find that measured wave levels do not agree with the prediction from the theory based on the nonlinear saturation of the beam-plasma interaction producing the wave [Cairns and Gurnett, 1990-1991].

Frequency Spectrum:

Measurements show that most strongly excited waves occur in the near vicinity of the spacecraft within a distance of about 30 m from it. Figure 16 shows the frequency spectrum of the electric field in this so- called near zone. The spectrum is generally confined to frequencies below the lower-hybrid frequency defined by

$$f_{lh} \simeq \sqrt{f_{ce} f_{ci}} \tag{54}$$

where f_{ce} and f_{ci} are the electron and O^+ cyclotron frequencies, respectively. Above this frequency, the spectrum falls off abruptly. The typical value of $f_{lh} \simeq 5$ kHz. On occasions, well-defined peaks are found in the frequency spectrum; the peak near 178 Hz and f_{lh} are noteworthy [Cairns and Gurnett, 1991], at occasions even peaks at a frequency $2f_{lh}$ have been also observed.

Electric Field Amplitude:

In connection with EMI, in addition to the frequency spectrum, the electric field amplitude in an important quantity. Murphy[1987] attempted to correlate the electric field amplitude with the gas emission rate, using data on waves from PDP. figure 17 shows the variation of the rms electric field at 1 kHz within a bandwidth of 150 Hz, as a function of the gas emission rate G_r. Note that the emitted gas is mostly H_2O vapor. Performing a curve fitting, we find that the rms field (E_{rms}) is given by

$$E_{rms} \simeq 2.5 G^{\alpha} \quad mV/m \tag{55}$$

where α is an exponent between 0.7 and 0.8, and G^{α} is the gas emission rate in gram/s. The

gas density n_W can be related to the gas emission rate by

$$n_W \simeq \frac{G}{V_o \pi r^2 sin^2\theta} \tag{56}$$

where V_o is the gas ejection velocity from a nozzle of half-angle θ and r is the distance from it.

Since the contaminant number density is proportional to the gas emission rate, it is suggested here that $E_{rms} \alpha n_{w+}^{\alpha}$, n_{W+} being density of water ions in the vicinity of the spacecraft. The water ion density is expected to vary linearly with the gas density n_W.

Recent studies show that observed waves are best described by wave modes driven by water ion beam travelling with the orbital velocity of 8km/s, perpendicular to the earth's magnetic field, in the ionospheric O^+ plasma [Cairns and Gurnett, 1991]. The waves propagate nearly perpendicular to the magnetic field, and have a wavelength given by $\lambda = 2\pi/k$, where wavenumber k = w_{po}/V_{orb} where w_{po} is the oxygen ion plasma frequency, and V_{orb} is the orbital velocity of the spacecraft. for the ionospheric plasma density in the range $10^{11} - 10^{12} m^{-3}$, the wavelength range is 3-1m. The water-ion beam driven instability adequately describes the observed frequency spectrum discussed earlier. This instability has been extensively studied in a laboratory plasma and a thorough discussion can be found in Seiler [1977].

The real challenge here is to theoretically estimate the wave amplitude level, which can adequately describe the observational result in (55), namely, $E_{rms} \alpha n_{w+}^{\alpha}$, where α is in the range 0.7 to 0.8. Since the linear instability is driven by a beam, and beam velocity $V_{orb} \gg$ the thermal velocities of O^+ and H_2O^+ ions, the instability is likely to be saturated by trapping the beam ions in growing potential wells of the excited waves [Seiler, 1977]. A summary of the theory of wave saturation in beam-plasma system can be found in Hasegawa [1975]. the

linear dispersion relation for the waves is given by [Cairns and Gurnett, 1990,1991]

$$1 - \frac{n_o}{n_e}\frac{\Omega_{lh}^2}{\omega^2} - \frac{n_w}{n_e}\frac{\Omega_{lh}^2}{(\omega - k_\perp V_{orb})^2} = 0 \tag{57}$$

where $\Omega_{lh} = 2\pi f_{lh}$, ω is the wave frequency, n_o, n_W and n_e are the density of oxygen and water ions, and electrons, respectively. A detailed derivation of this equation can be found in Cairns and Gurnett [1990]. Here we have written the dispersion relation in the rest frame of the ionospheric plasma. Drawing an analogy between the standard dispersion relation for a beam-plasma system and the above equation, the solution for the wave with maximum growth rate can be written as follows:

$$k_\perp = (\frac{n_o}{n_e})^{1/2}\Omega_{lh}/V_{orb} \tag{58}$$

$$w = (\frac{n_o}{n_e})^{1/2}\Omega_{lh}(1 - \delta) \tag{59}$$

$$\delta_r = 2^{-4/3}(n_W/n_o)^{1/3} \tag{60}$$

$$\delta_i = -\delta_r/\sqrt{3} \tag{61}$$

Where δ_r and δ_i are the real and imaginary part of (δ). The wave phase velocity is given by

$$V_p = w_r/k_\perp = (1 - \delta_r)V_{orb} \tag{62}$$

where $w_r = R_e(w)$. In the rest frame of the wave phase velocity, ions have a relative speed given by

$$\triangle V_p = V_{orb} - V_p = \delta_r V_{orb} \tag{63}$$

Thus, in a growing potential of the wave, the beam ions begin to trap when the wave peak potential (ϕ_p) becomes large enough so that

$$2q\phi_p > \frac{1}{2}m_\omega \triangle v_p^2 \tag{64}$$

When the trapping begins, the beam ions begin to reflect back and the minium beam velocity is reached half a bounce time later. this minium beam velocity

$$U_{bmin} = v_p - \triangle v = V_{orb} - 2\delta_r V_{orb} \tag{65}$$

Note that the initial beam velocity without the wave is V_{orb}. the reduced beam velocity indicates that the kinetic energy of the beam has been converted into wave energy. half of this wave energy goes into the electrostatic energy, while the other half goes into the plasma particles. We are concerned here with the electrostatic part of the energy and the corresponding electric field. The time average electrostatic energy

$$W_e = \frac{1}{4}\epsilon_o |E_{max}|^2 = 2\delta_r(1-\delta_r)(\frac{1}{2}n_\omega m_\omega V_{orb}^2) \tag{66}$$

and the corresponding field is

$$|E_{max}| = 2^{\frac{5}{3}}(\frac{n_\omega}{n_o})^{1/3}[1-2^{-4/3}(n_\omega/n_o)^{1/3}][\frac{1}{2}n_W m_w V_{orb}^2] \tag{67}$$

Table 1 shows the value of $|E_{max}|$ for two ionospheric plasma densities , $n_o = 10^{11}$ and $10^{12}m^{-3}$, and for water ion densities ranging from 0.2×10^{10} to $10^{10}m^3$. It is seen that the fields up to a few tens of volts/m are likely to be generated. We recall that such fields are generated near the lower hybrid frequency, which is about 5 kHz in the low earth orbit.

The large electric field calculated above occurs at a very short time scale just after the water vapor is released. We estimate here this time scale. The saturation state is characterized by oscillations having frequencies determined by the bounce motion of the trapped ions in the evolving field [Hasegawa, 1975]. The bounce frequency is given by

$$\omega_b = (\frac{ek_\perp E}{m_w})^{\frac{1}{2}} \tag{68}$$

Using the $k_\perp$ in (58) and E_{max} for E, $n_W = 10^{10}m^{-3}$ and $n_o = 10^{11}m^{-3}$, we estimate $k_\perp \simeq$ 0.6m, E = 51 V/m, $w_b = 1.3 \times 10^4$ rad/s, and the bounce period

$$T_b = \frac{2\pi}{w_b} \approx 0.5 \quad ms \tag{69}$$

$n_o = 10^{12} m^{-3}$

n_W	0.2×10^{10}	0.4×10^{10}	0.6×10^{10}	0.8×10^{10}	0.1×10^{11}
E(V/m)	18.3	28.7	37.1	44.5	51.3

$n_o = 10^{12} m^{-3}$

n_W	0.2×10^{10}	0.4×10^{11}	0.6×10^{10}	0.8×10^{10}	0.1×10^{11}
E(V/m)	12.9	20.3	26.5	32.0	37.0

Table 1: Maximum electric fields in Volt/meter for several values of water ion density (n_W) and for two typical values of oxygen ion density n_o

The large electric fields estimated here should last over a few bounce periods., i.e., only for a few milliseconds after the gas release.

At times later than several milliseconds, a very different set of non- linear process are likely to occur. Such processes spread the plasma waves to lower frequencies making a broadband electrostatic noise. The observed spectrum of the noise belongs to this relatively late stage of the instability. This stage is difficult to analytical estimate and best way to obtain quantitative estimates is to perform numerical simulations. Such simulation studies are beyond the scope of this work. However, a crude estimate can be made as follows. When the beam is almost completely thermalized, the electric field energy density integrand over the entire frequency spectrum is given by

$$W = \int \frac{1}{2}\epsilon_o |E_w|^2 = (\frac{n_w}{n_o} n_o k_B T \simeq n_w T \tag{70}$$

where $|E_w|^2$ is the power spectral density, T is an effective temperature and k_B is the Boltzmann constant. In view of the observed spectrum of the broadband noise, we assume that the noise is uniformly distributed over the bandwidth $\triangle f \sim f_{lh}$,starting from zero frequency. Thus, the spectral power density is

$$|E_w|^2 = \frac{2 n_w T}{4 \triangle f \epsilon_o} \quad V^2 m^{-2} Hz^{-1} \tag{71}$$

Observation indicates a typical value of $n_w \simeq 0.1 n_o, n_o \simeq 10^{11} m^{-3}$ and $\triangle f \simeq 10^4$ Hz. We do not know the value of T precisely because the beam is likely to heat the plasma. If this heating is ignored, T$\simeq$0.1 eV and $|E_w|^2 \simeq 3.6 \times 10^{-3} V^2 m^{-2} Hz^{-1}$, and the corresponding electric field in a 150 Hz band, as in Figure 17, is about 700 mV/m. this field is about an order of magnitude larger than the observations indicate. It is worth mentioning that, the observed fields can be an underestimate due to the antenna size as pointed out by Cairns and Garrett [1990].

In summary, we emphasize that the gas releases can generate electric fields up to several tens of volts/m near the lower hybrid frequency. Such strong fields cascade downward and upward to lower and higher frequencies, which are measured. however, in the late stage of the instability too, the analytical estimates are found to be considerably higher than measured fields. In view of this discrepancy, a better estimate based on numerical simulations and also an estimate of the effect of antenna size on the measurements of the fields are needed.

8 Radiation of EM Waves by Currents Induced in the Structure by the Motional EMF

The motional EMF in a moving conductor at the altitudes of the Space Station can be as large as $0.3Vm^{-1}$. Assuming a length of about 100 m (as that of the keel), an estimate of the maximum possible EMF is about 30 volts. The induced EMF can drive a current through the structure, but the current drawn is critically controlled by the ambient plasma and its contact with the structure. These are difficult unsolved problems. However, the current collection at the positive end involves the collection of electrons, while at the negative end the collection of ions. Since the ion thermal current density in the ambient plasma is considerably smaller than the electron current density, the ions are likely to dictate the current in the structure. If the ion current collection area at the negative end is S_i, the current flow through the structure is approximated by

$$I = J_i S_i \tag{72}$$

where J_i is the ion current density in the range $n_o e V_{ti} < J_i < n_o e V_S$, V_{ti} is the ion thermal velocity,V_S is the Space Station velocity, n_o is the ambient plasma density, and e is the magnitude of the electronic charge. The upper limit on the ion current density J_i is determined by the ram current, while the lower limit is by the ion thermal motion. Thus, the maximum possible power available for radiation is given by

$$P = V_s B L J_i S_i \tag{73}$$

The ion current density with the ambient plasma density $n_o = 10^5 cm^{-3}$ and ion temperature of 0.3eV is found to be in the range $10^{-4} Am^{-2} > J_i > 3 \times 10^{-5} Am^{-2}$. Thus, the radiated power is found to be

$$9 \times 10^{-4} S_i < 3.3 \times 10^{-3} S_i \quad watts \tag{74}$$

Assuming S_i to be about $500m^2$, the radiate power lies in the range 0.45 watts <P<1.65 watts. This estimate of power, based on intuitive arguments, is approximately the same as obtained by more rigorous calculations [Chlouber, 1987].

Now let us consider the frequency range over which the power will be distributed. The radiation occurs at frequencies given by

$$f = k.V_s/2\pi \quad Hz \tag{75}$$

where k is the wave vector of the radiation. Since maximum possible value of k in a plasma is roughly λ_d^{-1}, the highest radiated frequency is given by

$$f \simeq \frac{1}{2\pi}\frac{V_s}{\lambda_d} \simeq f_{pe}\frac{V_s}{V_{te}} = f_{pi}\frac{V_s}{V_{ti}} \tag{76}$$

where f_{pi} and f_{pe} are the ion and electron plasma frequencies and V_{ti} and V_{te} are the ion and electron thermal velocities.

At the altitudes of Space Station $f_{pi} \simeq 23.4kHz$ and $f_{lh} \simeq 5.4kHz$. Thus, a variety of wave modes are likely to be expected; these include Alfven waves, electromagnetic ion-cyclotron mode, ion-acoustic mode, ion Bernstein waves, and lower hybrid waves.

Whether a given mode is radiated or not also depends on the wavelength spectrum of the current source in the structure. If some wavelengths are not in the source, they are not radiated, even if the plasma allows such a radiation.

The component of k parallel to the velocity of the structure is relevant here. Thus, if the dimension of the structure in the direction of the motion is L_v, the typical radiated wave number is given by

$$k_v < L_v^{-1} \tag{77}$$

and the radiated frequency

$$f_o < \frac{1}{2\pi}V_s/L_v \tag{78}$$

Since $V_s \simeq 7.3 kms^{-1}$ and $L_v \approx 5m$, $f_o < 230Hz$. Thus, the Space Station structure is likely to curtail the radiation in frequencies higher than about 230 Hz. This frequency is lower than H^+ cyclotron frequency, but several times larger than O^+ and H_2O^+ cyclotron frequencies. thus, the possible wave modes are Alfven waves, electromagnetic ion-cyclotron waves, ion-acoustic waves, and O^+ Bernstein modes. The latter two waves are warm plasma affects.

The warm plasma effects on the radiation from structures in space have not been investigated at all. Longitudinal plasma waves may have important ramifications as they heat the plasma near the source. Heating involves Landau damping and/or ion-cyclotron damping.

Since the plasma waves are likely to be damped near the structure, the radiated power away from it will be primarily in the form of Alfven waves. The electric field strength of the Alfven waves is approximately

$$E \simeq (\mu_o V_a \frac{P_a}{S})^{\frac{1}{2}} V m^{-1} \tag{79}$$

where V_a is the Alfven velocity, S is cross section of the space Station perpendicular to the ambient magnetic field, μ_o=4 $\pi \times 10^{-7} Hm^{-1}$ and P_a is the power in Alfven waves.

Assuming P_a = 1 watt and S = $10^3 m^2$, V_a = 200 km s^{-1}, E$\simeq$ 16 mVm^{-1} and B = 80 nT. The electric field strength given above is roughly comparable to the requirement given in Figure 3.1-3 of JSC 30420. But the corresponding B field specifications are much lower than the estimate given above.

Conclusion:

The main point of this report are as follows.

The capacitances in the system critically control the effect of arcing on the power system. If the capacitances are sufficiently large, they act like low impedances during the arc rise time and hence a large fraction of the arc current is likely to flow into the power system. This implies a significant perturbation in the operation of the solar cells, especially those at negative potentials before the onset of an arc.

It is recommended that accurate estimates be made for the capacitances including the capacitance of the solar cells to plasma and also the anticipated capacitive load on the system.

If the arc current is injected into the plasma and a significant fraction of the injected electrons escape along the earth's magnetic field, the radiation fields confined in narrow cones emanating from each arc can be significant. A firm understanding of the charge neutralization processes and of the dynamics of the electrons ejected during arcing is needed to decisively address the EMI effects created by arcing.

If a significant fraction of electrons ejected during escape along the magnetic field line, the radiation losses are so great that the arcing current is limited. Estimates show a limit $\approx$200 A on arc current by the radiation loss alone.

If the arcing process limits the escape of electrons, the local current near the arcing spot in the plasma is likely to radiate intense plasma waves, which are absorbed by the electrons and ions. In turn, the plasma is heated. If the SSF structure is likely to heat the plasma to about 100 eV in the close vicinity of SSF. Such a heating has a direct bearing on the behavior of the materials used for the structure.

If plasma contactors are used to control the charging of the SSF structure, the plasma wave generated by electrons ejected by the contactor currents ($<$1A) may not be directly of

concern for EMI. however, such plasma waves may interrupt the contactor currents, leading to the charging of the structure and possible arcing. It is recommended that if the charging is to be controlled using contactors, their stability, especially dealing with the intensity of the current interruptions be firmly established.

References

Hasegawa, A, Plasma Instability and nonlinear Effects, Springer-Valag,Berlin,Chapter 4, 1975

Balmain, K.G. The impudence of short dipole antenna in a magnetoplasma, *IEEE Trans. on Antennas and Prop.*, pp 605-617, 1964

Cairns, I.H., and D.A. Gurnett, Plasma waves observed in the near vicinity of the Space Shuttle, *J. Geophy. Res.*

Cairns, I.H., and D.A. Gurnett, Plasma waves associated with the Space Shuttle, ESA sp-311, p.87, August, 1990

Cairns, I.H., and D.A. Gurnett, Control of plasma waves associated with the space shuttle by the angle between the orbit's velocity vector and the magnetic field, J.Geophy. Res.,96,7591,1991.

Chlouber, D.E., Space Station Induced Electrical Noise and Drag Interaction, McDonnel Douglas Astronatic Corp., Houston Div., TM No. 528-005-1, 1987.

Davis, V.A., I. Katz, M.J.Mandell and D.E. Parks, Hollow Cathodes as Electron Emitting Plasma Contactors: Theory and Computer Modeling, J. Spacecraft, 23,pp 175-179, 1988

Kellogg, P.J., S.J. Monson, W.Bernstein, and B.A. Whalen, Observation of waves generated by electron beams in the ionosphere, J. Geophys. Res., 91,12065,1986.

Kurth, W.S., Interperception of plasma diagnostic package results interms of large structure plasma interactions, Final Technical Report, NASA Lewis Res. Center Grant, NAG3-449, Aug.,1991.

Metz, R.N., Current transients due to arcs on a high-voltage solar array, J. Space craft, 23, pp 499-504,1986

Murphy, G.B., Contaminant ions and waves in the Space Station Environment, Space Station contaminants workshop proceedings, OSSA/NASA, Hilton Head, SC , Oct. 29-30, 1987

Neubert, T., S. Sasaki, B.E. Gilchrist, P.M. Banks, P.R. Williamson, A.C. Fraser-

Smith, and W.J. Raitt, Observations of plasma wave turbulence generated around large ionospheric spacecraft: Effect of motionally induced EMF and of electron beam emission, J. Geophy. Res., pp 9639-9654, 1991

Parks, D.E., I. Katz, Theory of Plasma Contactors for Electromagnetic Tethered Satellite Systems, J. Spacecraft,24, pp 245-249, 1987

Seiler, S.W., Linear and non-linear development of a lower hybrid wave driven by a perpendicular ion beam, Ph.D. Thesis, Princeton University, 1977

Singh, N. and R.W. Gold, Radiation from a short electric dipole in a hot uniaxial plasma, Radio Sci., 6, pp. 1151-1163, 1971

Singh, N. and B. I. Vashi. Current Collection by conducting bodies in the low earth orbit, AIAA 22nd Fluid Dynamics Plasma and Lasers Conference, June 24-26, 1991, Honolulu, Hawaii, AIAA paper # 91-1472

Ward,J.W., H.J.King, Mercury Hollow Cathode-Plasma Bridge Neutralizers, J. Spacecraft, 5, pp. 1161-1164, 1968

ADDENDUM TO THE FINAL REPORT
NASA/MSFC, CONTRACT#NAS8-36955
PI: Dr. N. Singh

During docking between the shuttle and the space station, there is some concern about electrostatic discharge (ESD). However,the reduced negative potential on the structure of the station due-to the operation of a plasma contactor and also the thin insulation on it reduce the possibility of ESD. This is simply because the exterior surfaces of each spacecraft are at a potential of about - 1 V with respect to the ionospheric plasma, and therefore there is no potential difference between them. When the spacecrafts approach each other and separation between them reduces to a few centimeters, the ionospheric plasma effects including the sheath formation giving the -1 V potential on the surfaces are lost. In this situation, the shuttle comes under the direct influence of the negative potential on the structure. If the approaching shuttle surface is conducting, the electric field between this surface and the station structure will increase, and depending on the potential on the latter, discharge and arcing may occur. This situation is similar to that treated in section 2, except for some minor modification to include the capacitance between the shuttle and the space station in the discharge circuit of Figure 2. However, before such an analysis is performed, it is essential to clearly define the properties of the approaching surfaces during docking.

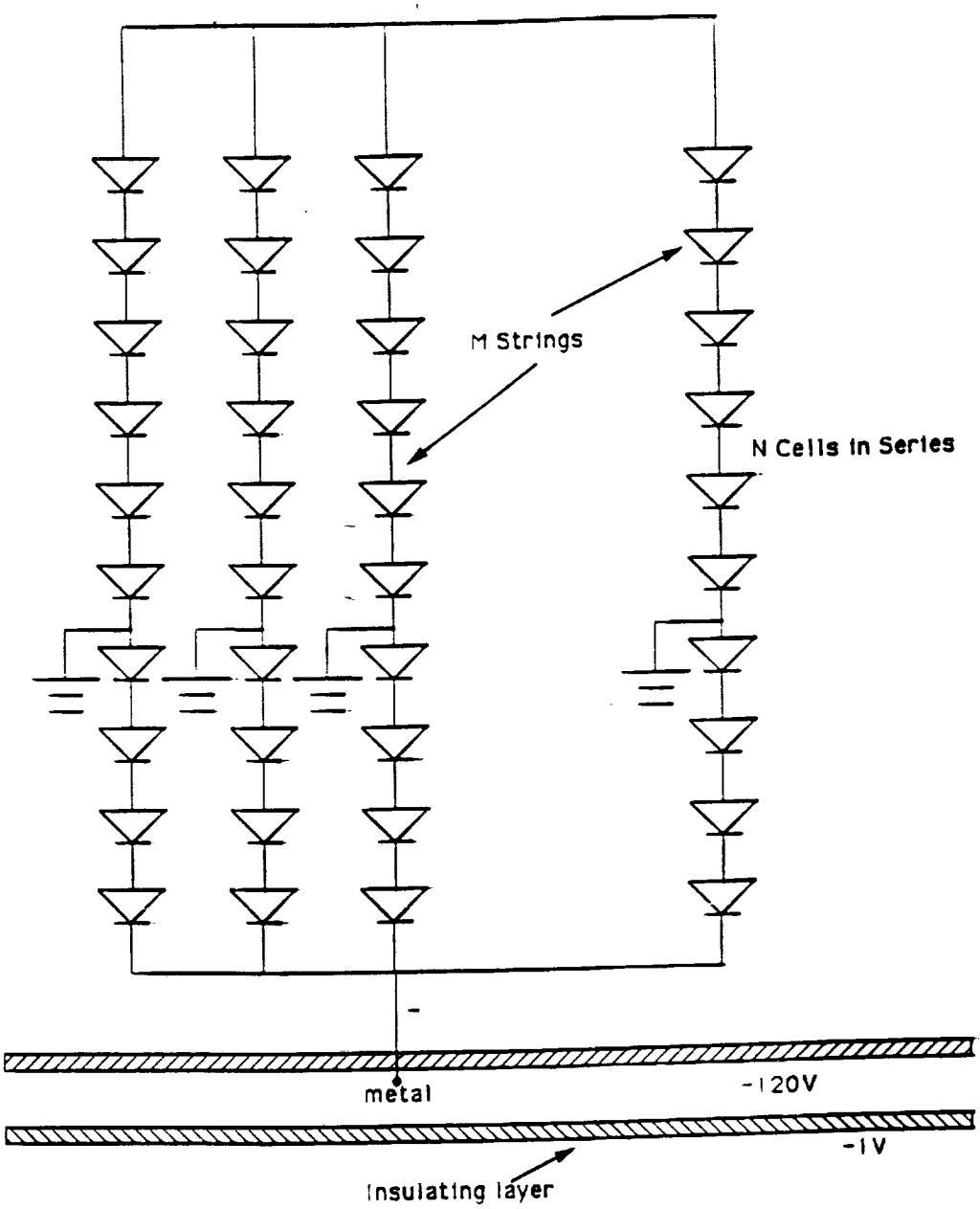

Figure 1 Schematic diagram showing the electrical connection of the negative end of the solar cell array with the structure of the Space Station Freedom. The structure consists of Al insulated with Al_2O_3.

R_A = 21 mΩ

R_I = 0.3 Ω

R_E = 65.1 Ω

R_I = 679.3 Ω

C_I = 1.47×10^{-5} F

C_E = 1.28×10^{-6} F

$R = R_R = R_S = 1 \times 10^{-8}$ Ω

$C_A \cong 6$ μF

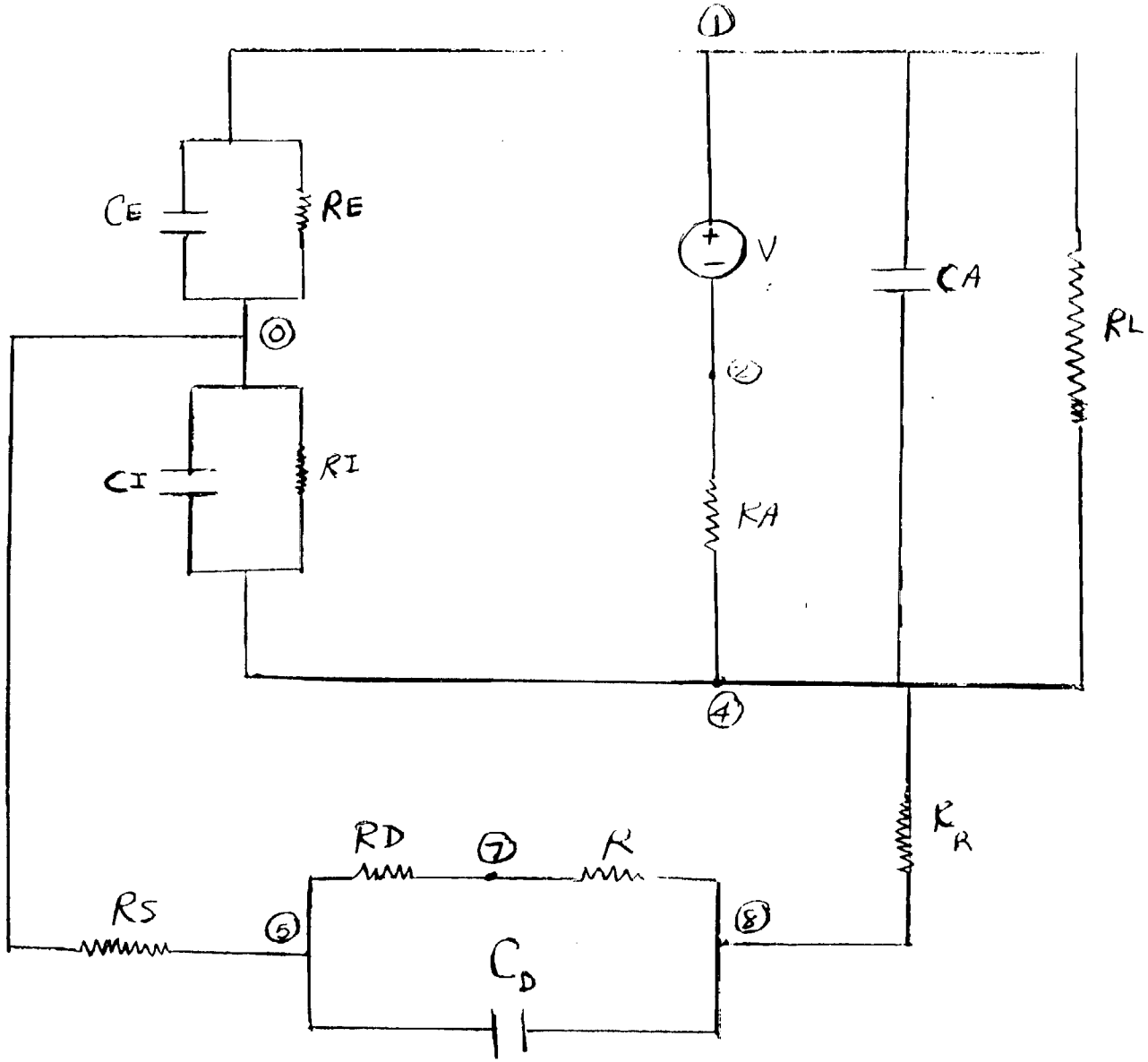

Figure 2 Circuit model for the SSF consisting of the solar cell array (V_A, R_A and C_A), the load (R_L), coupling between plasma and the array (C_E,R_E, C_I, and R_I), and the structure capacitance (C_D) and the discharge resistance (R_D).

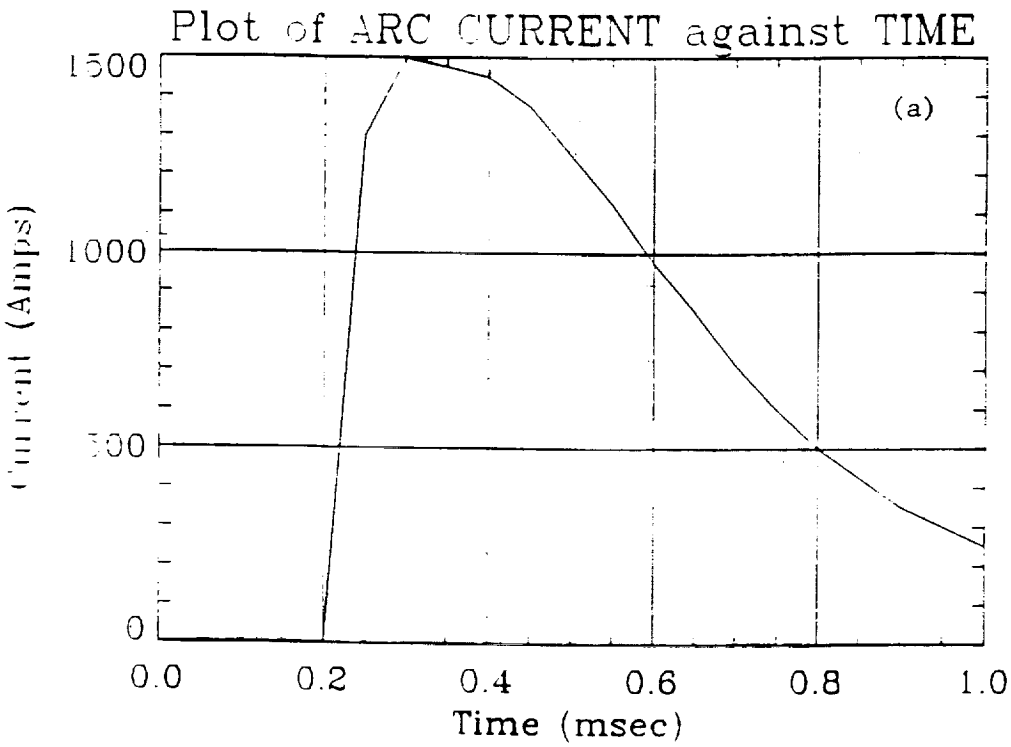

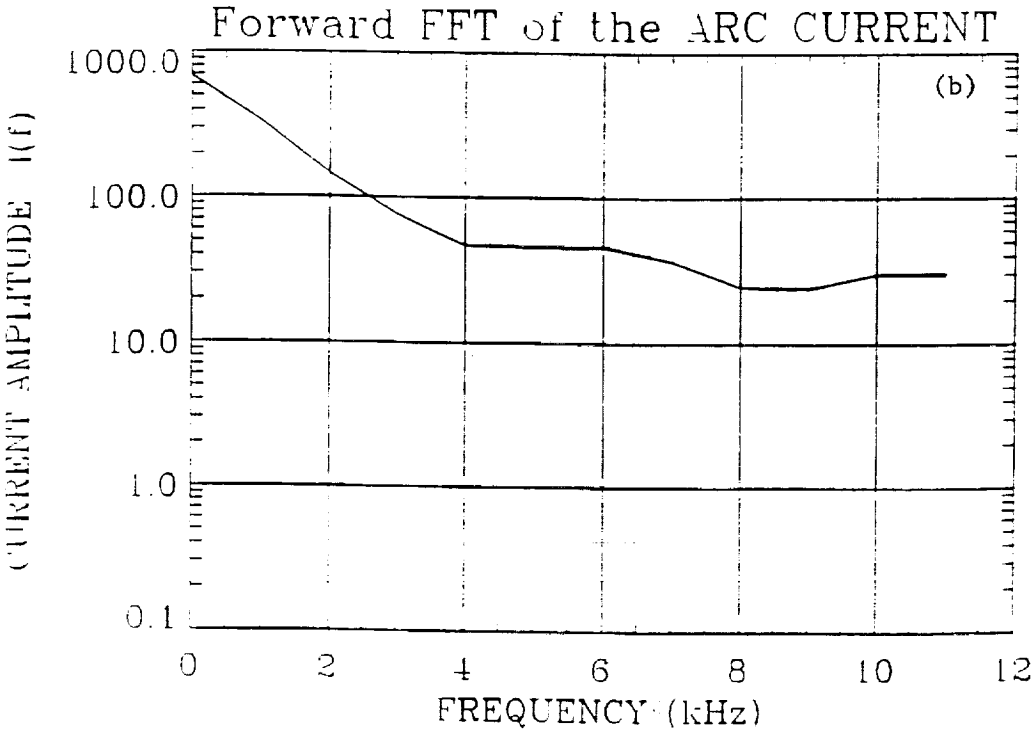

Figure 3 (a) An example of time history of an arc current (After Curruth, 1991)
(b) Fourier spectrum of the arc current.

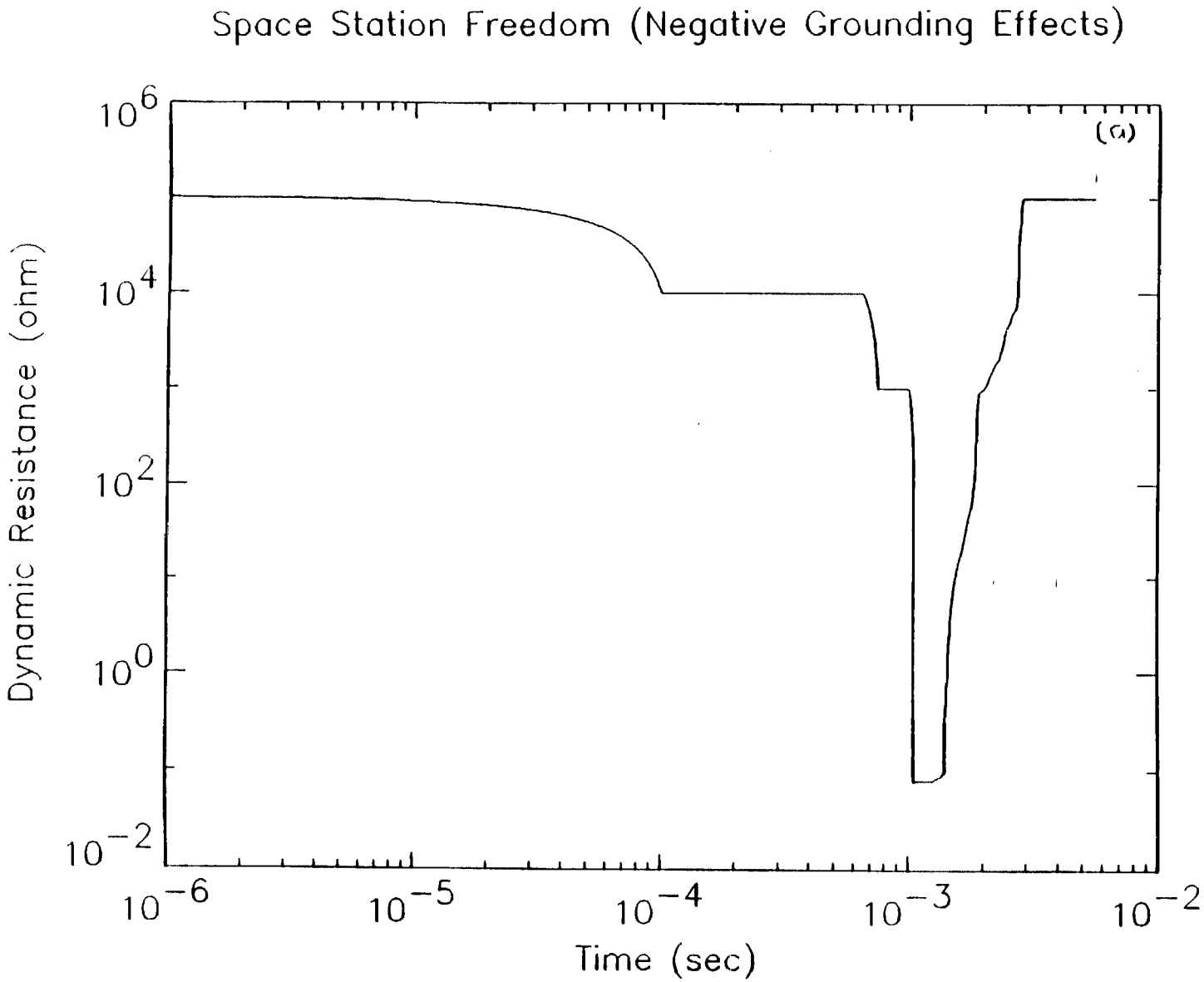

Figure 4 **(a)** **Temporal evolution of the dynamic resistance R_D.**
(b) **Simulated arc current through the loop consisting of C_D and R_D.**

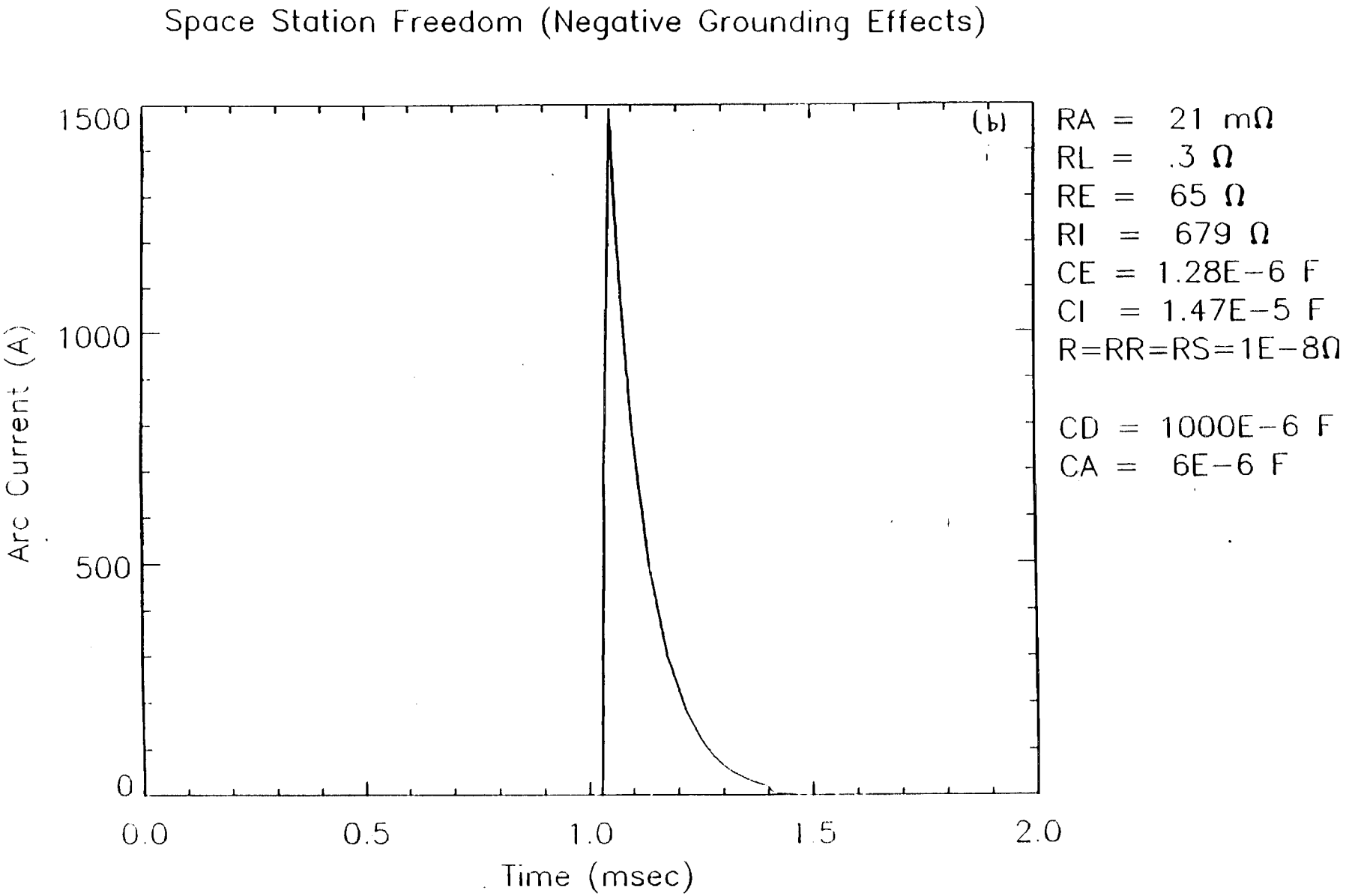

Figure 4b continued

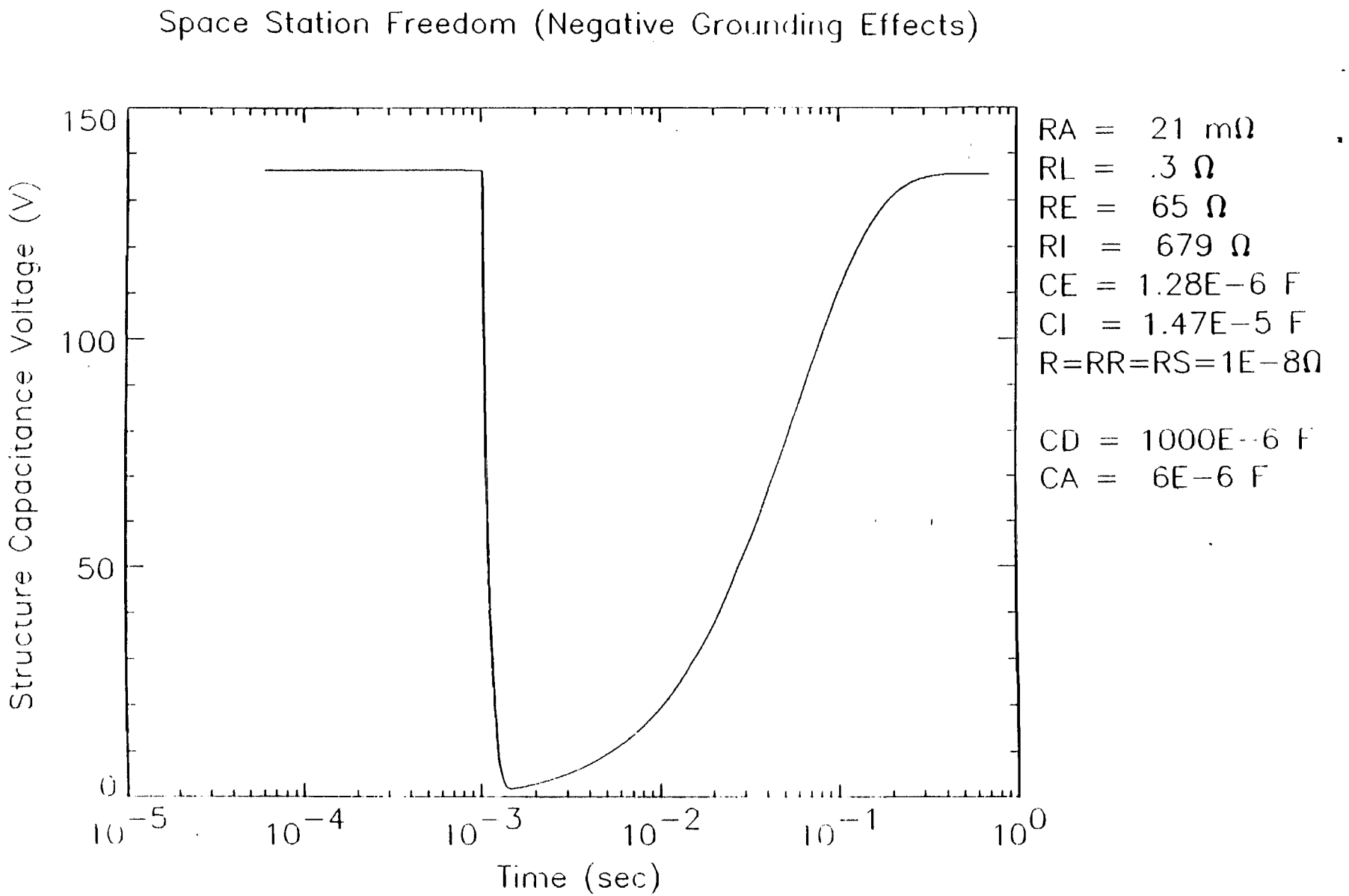

Figure 5 **Temporal evolution of the voltage across the structure capacitance C_D. Note that it takes about 200 ms for the structure to recharge again.**

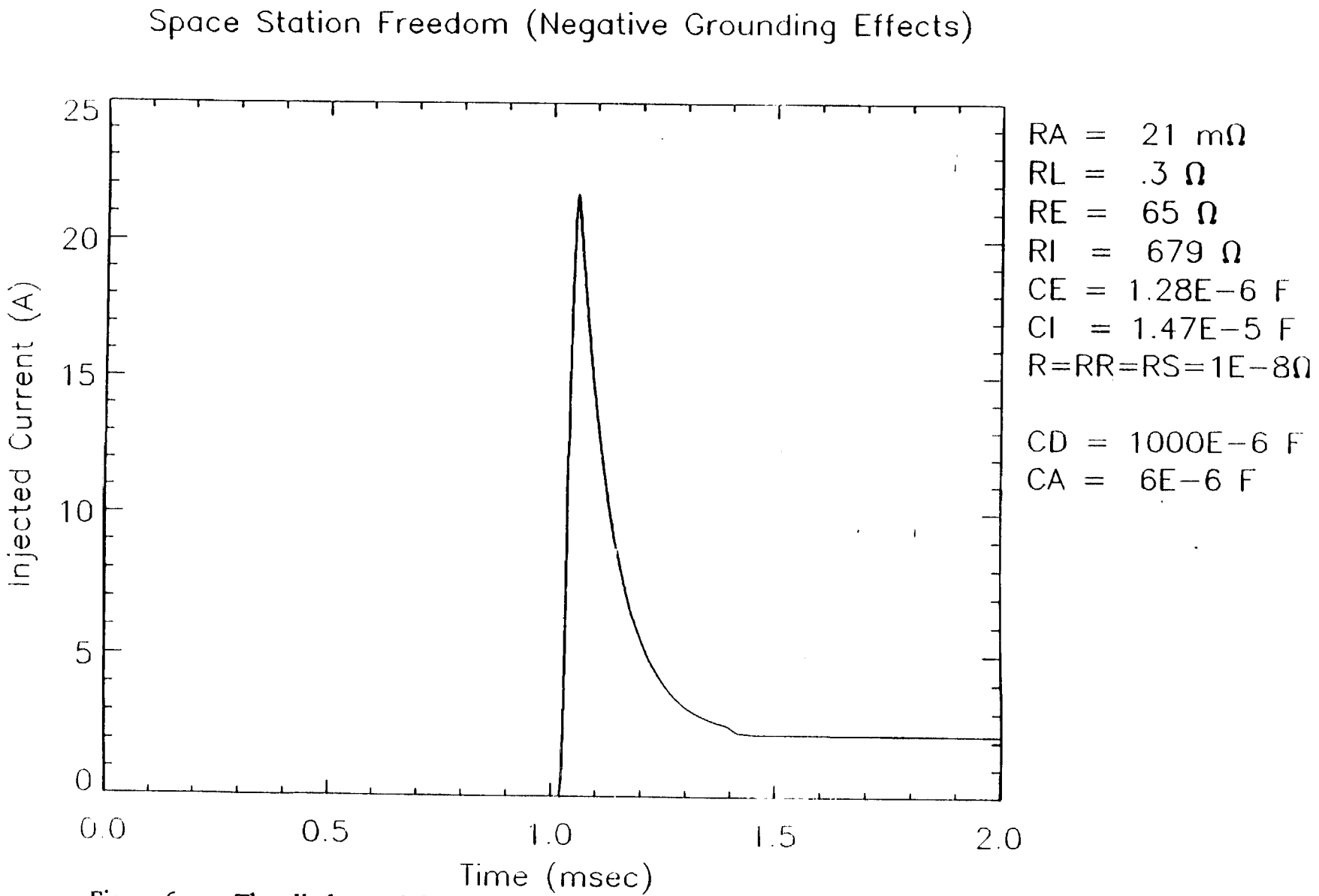

Figure 6 **The discharge injects a current into the main part of the circuit. The temporal evaluation of the current injected at the node 4 in the circuit of Figure 2.**

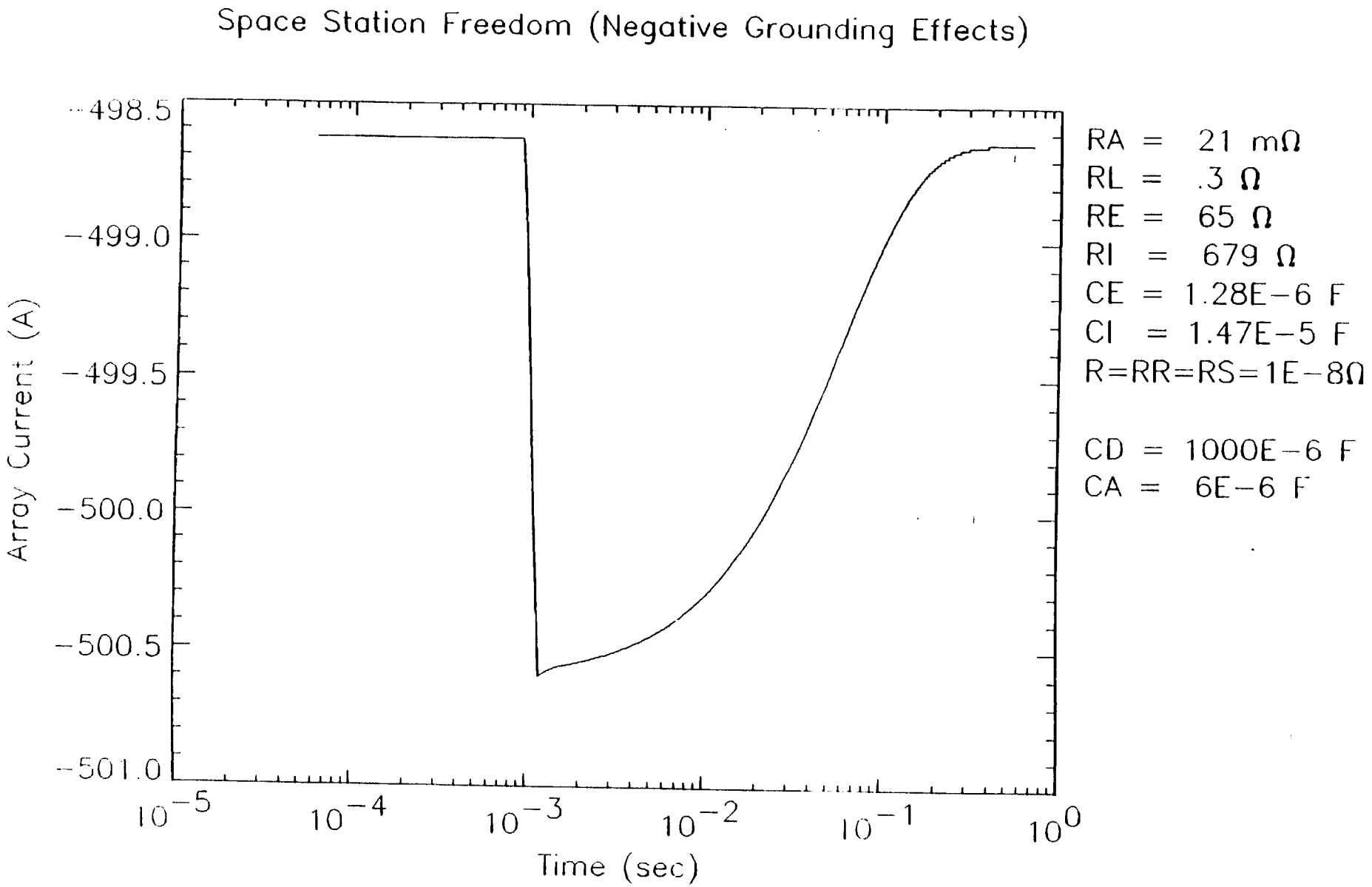

Figure 7 **Perturbation in the current through the solar cell array.**

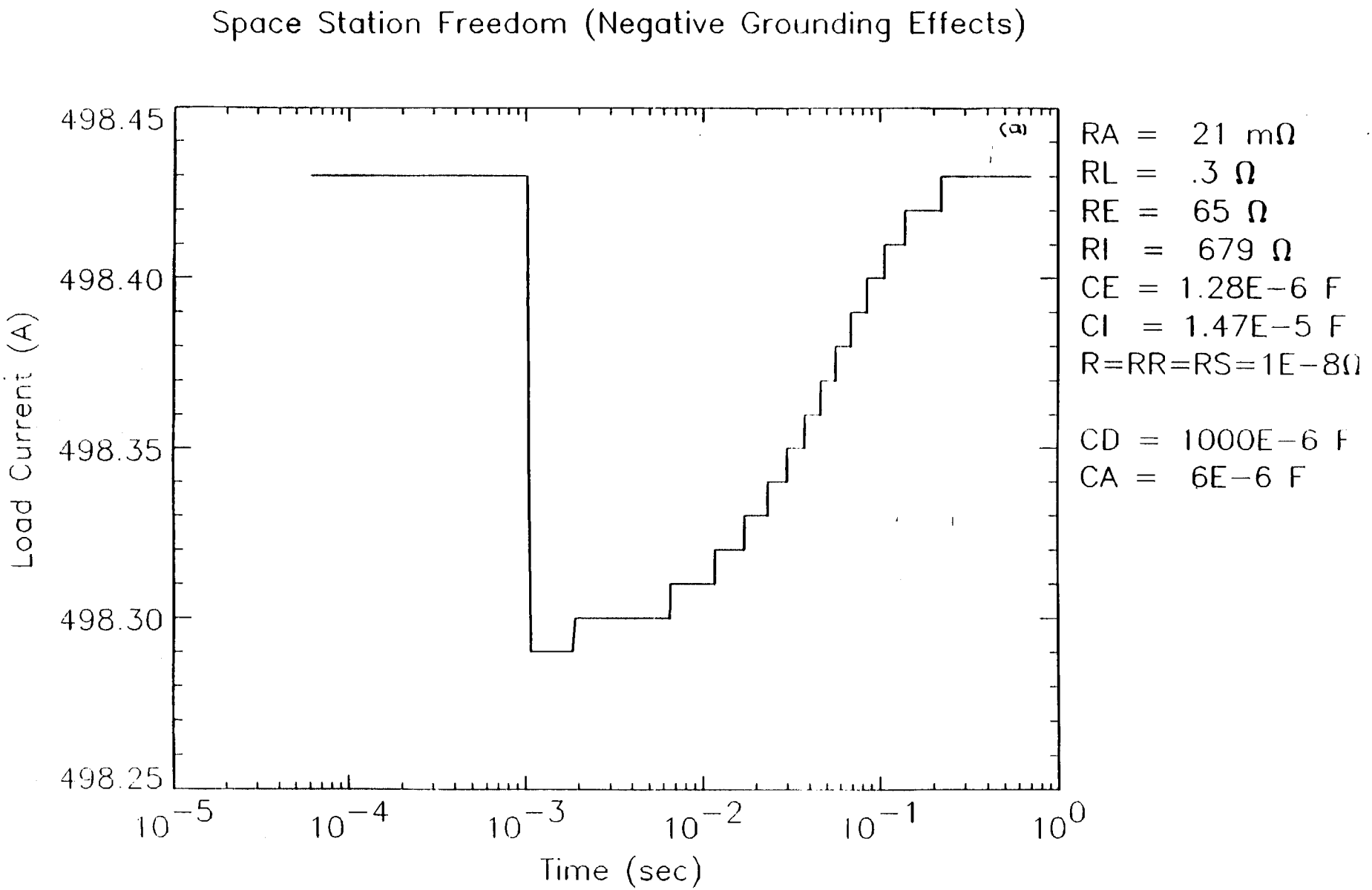

Figure 8 **Perturbations in the load**
(a) load current
(b) load voltage and
(c) load power.

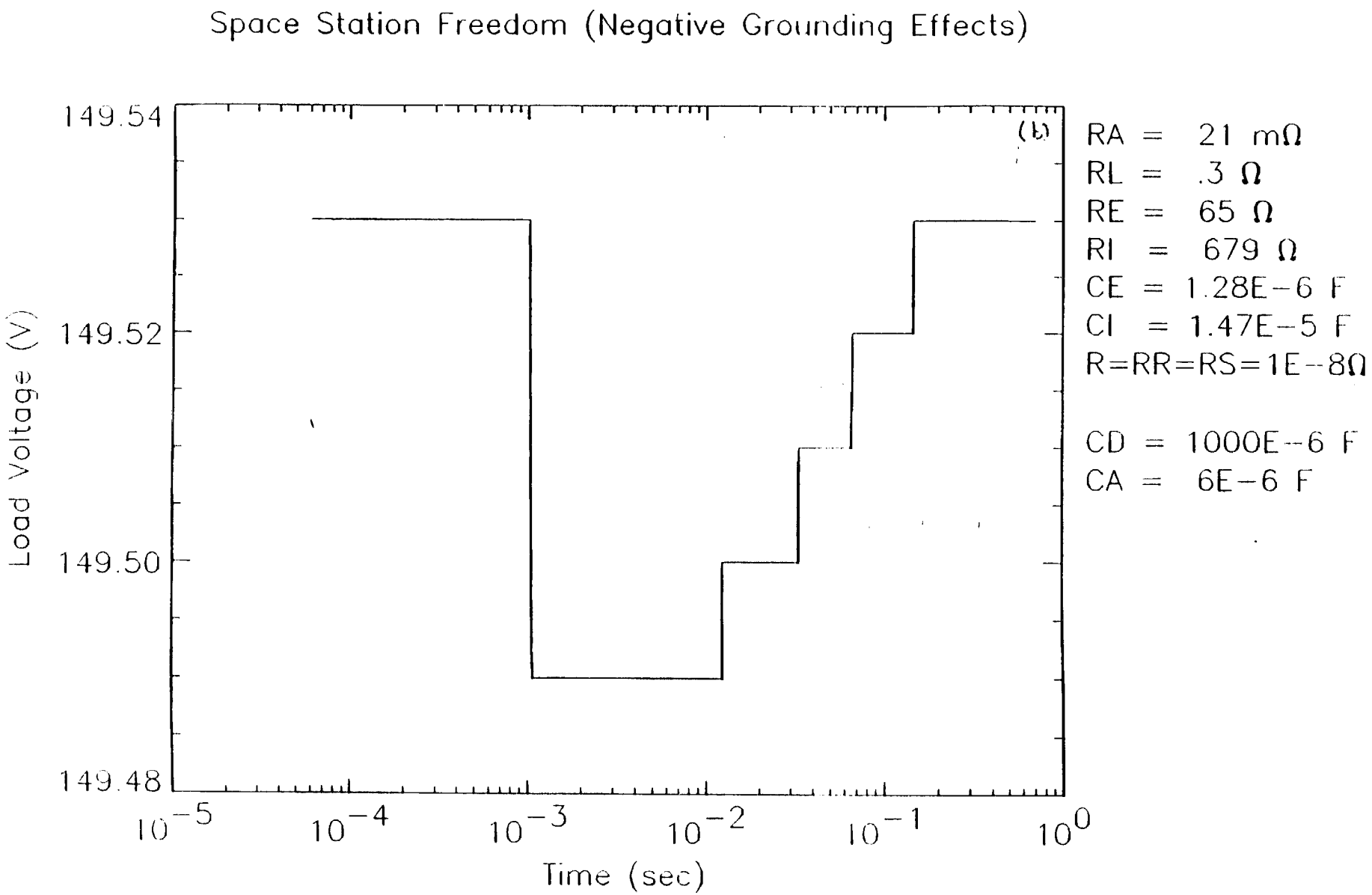
Space Station Freedom (Negative Grounding Effects)
149.54
149.52
149.50
149.48
Load Voltage (V)
(b)
RA = 21 mΩ
RL = .3 Ω
RE = 65 Ω
RI = 679 Ω
CE = 1.28E-6 F
CI = 1.47E-5 F
R=RR=RS=1E-8Ω
CD = 1000E-6 F
CA = 6E-6 F
10^{-5}
10^{-4}
10^{-3}
10^{-2}
10^{-1}
10^{0}
Time (sec)

Figure 8b

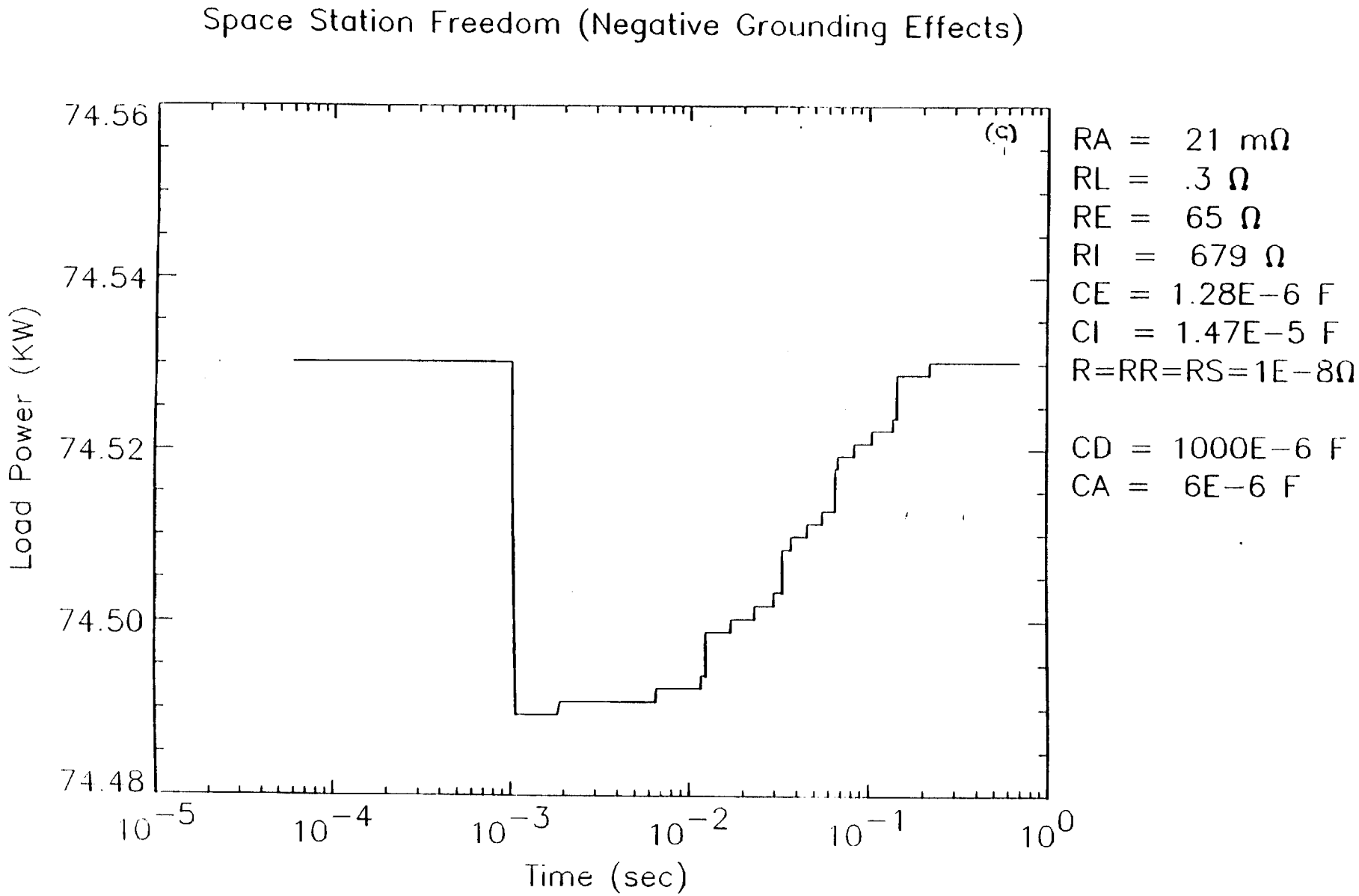
Space Station Freedom (Negative Grounding Effects)
(c)
74.56
74.54
74.52
74.50
74.48
Load Power (KW)
10^{-5}
10^{-4}
10^{-3}
10^{-2}
10^{-1}
10^{0}
Time (sec)
RA = 21 mΩ
RL = .3 Ω
RE = 65 Ω
RI = 679 Ω
CE = 1.28E-6 F
CI = 1.47E-5 F
R=RR=RS=1E-8Ω
CD = 1000E-6 F
CA = 6E-6 F

Figure 8c

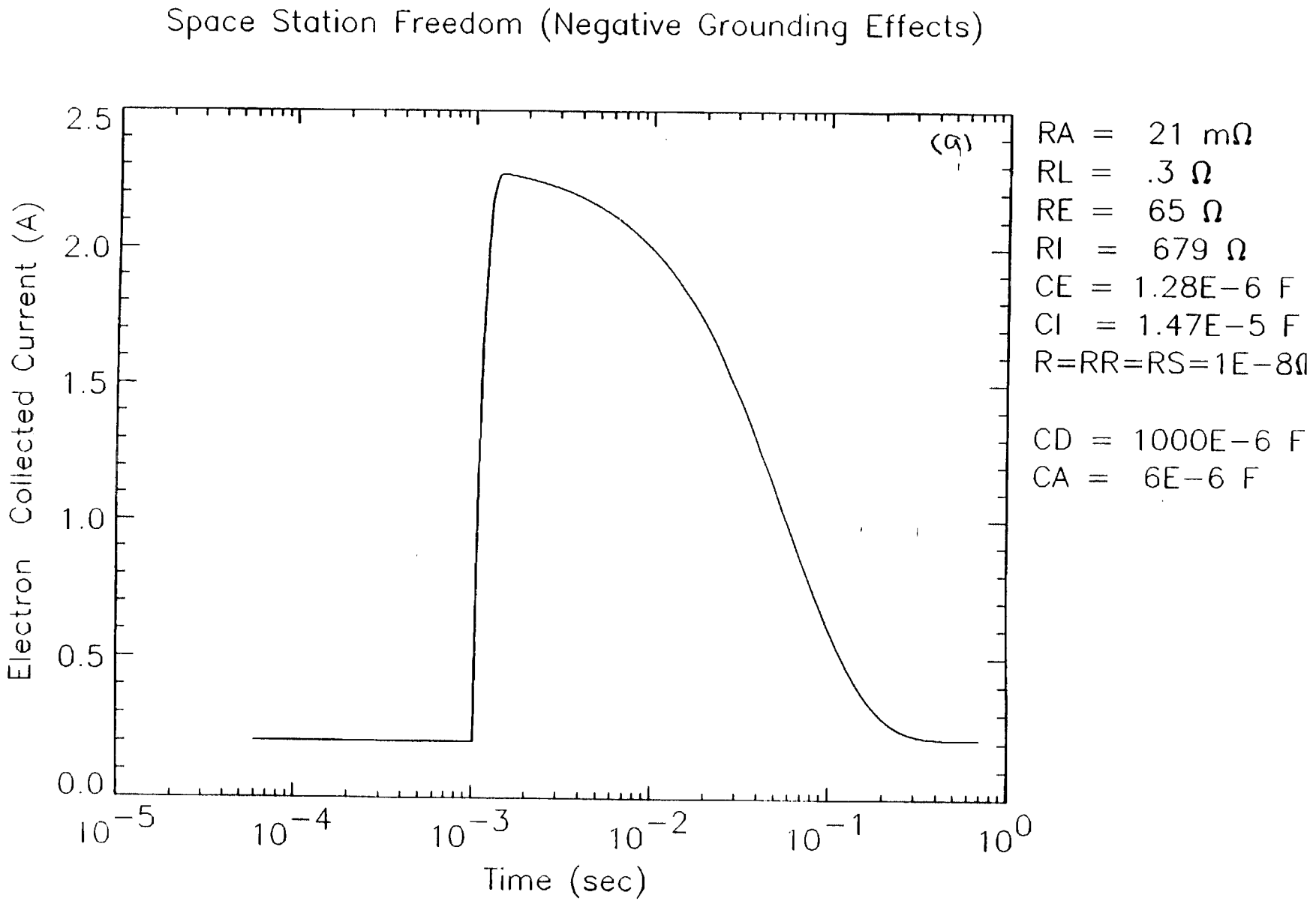

Figure 9 **(a)** Time history of current (I_E) through the resistance R_E
(b) Time history of current (I_I) through the resistance R_I

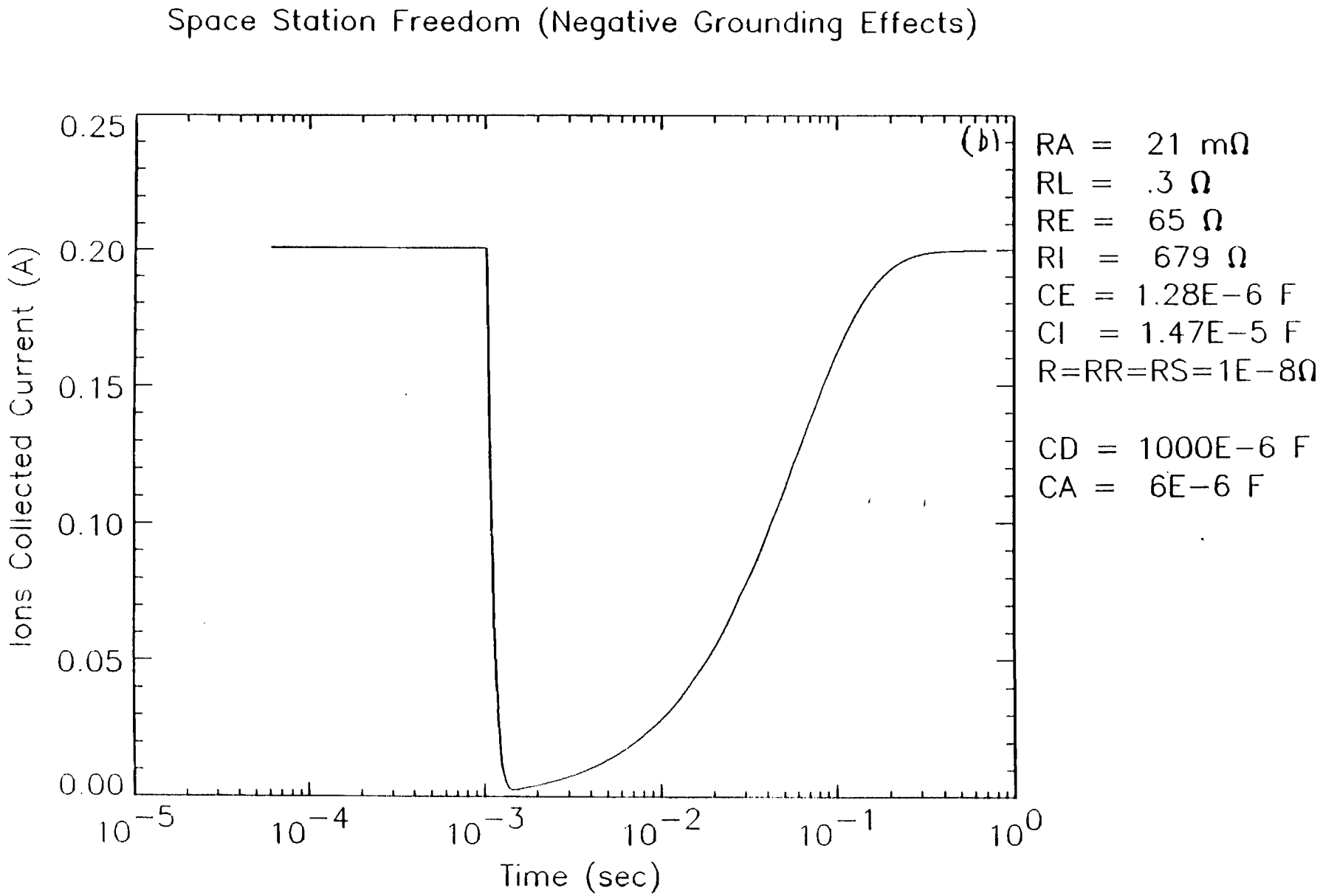
Space Station Freedom (Negative Grounding Effects)
(b)
RA = 21 mΩ
RL = .3 Ω
RE = 65 Ω
RI = 679 Ω
CE = 1.28E-6 F
CI = 1.47E-5 F
R=RR=RS=1E-8Ω
CD = 1000E-6 F
CA = 6E-6 F
Ions Collected Current (A)
0.25
0.20
0.15
0.10
0.05
0.00
10^{-5}
10^{-4}
10^{-3}
10^{-2}
10^{-1}
10^{0}
Time (sec)

Figure 9b

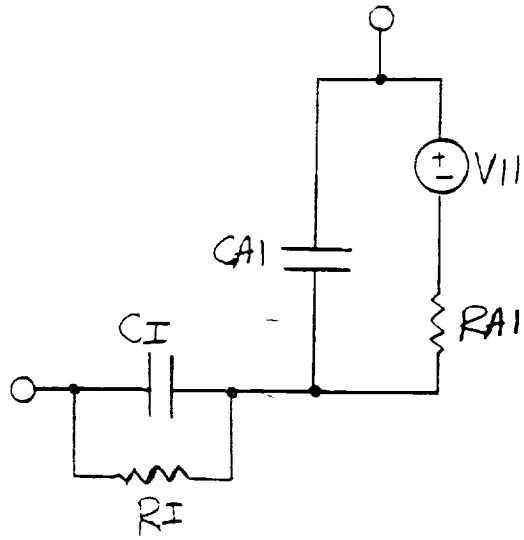

Figure 10 Equivalent circuit for a group of solar cells from the negative portion of the array.

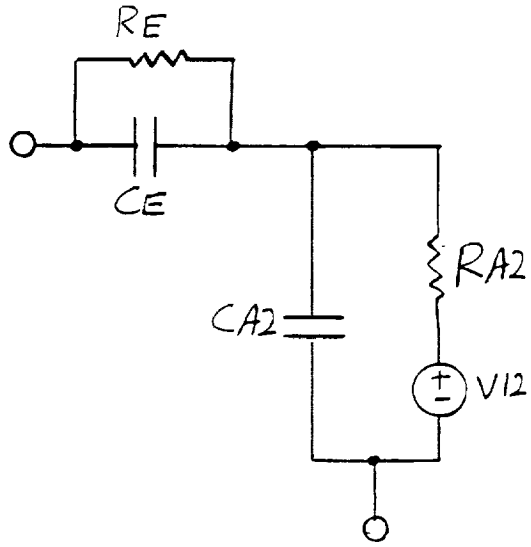

Figure 11 Equivalent circuit for a group of solar cells from the positive portion of the array.

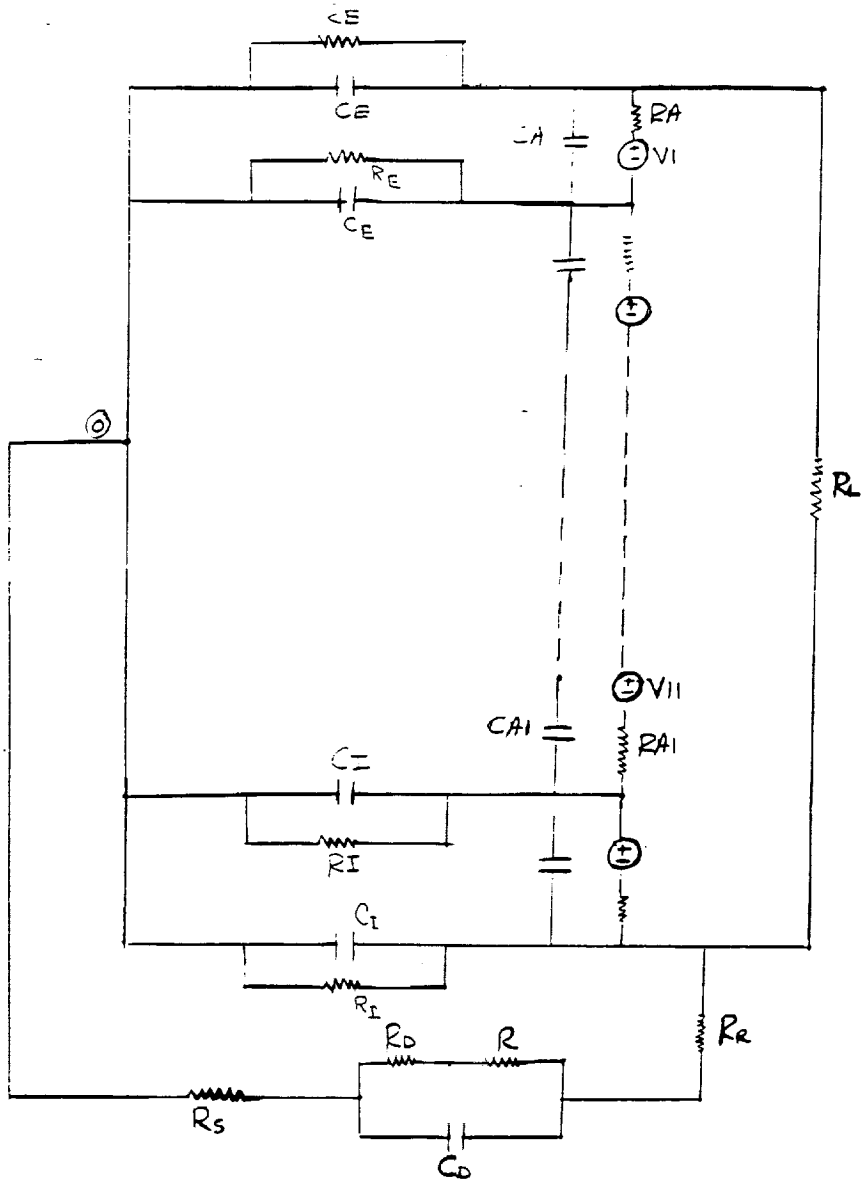

Figure 12 Distrubuted circuit model, in which solar cells and their equivalent capacitances and resistances to the plasma ground are grouped.

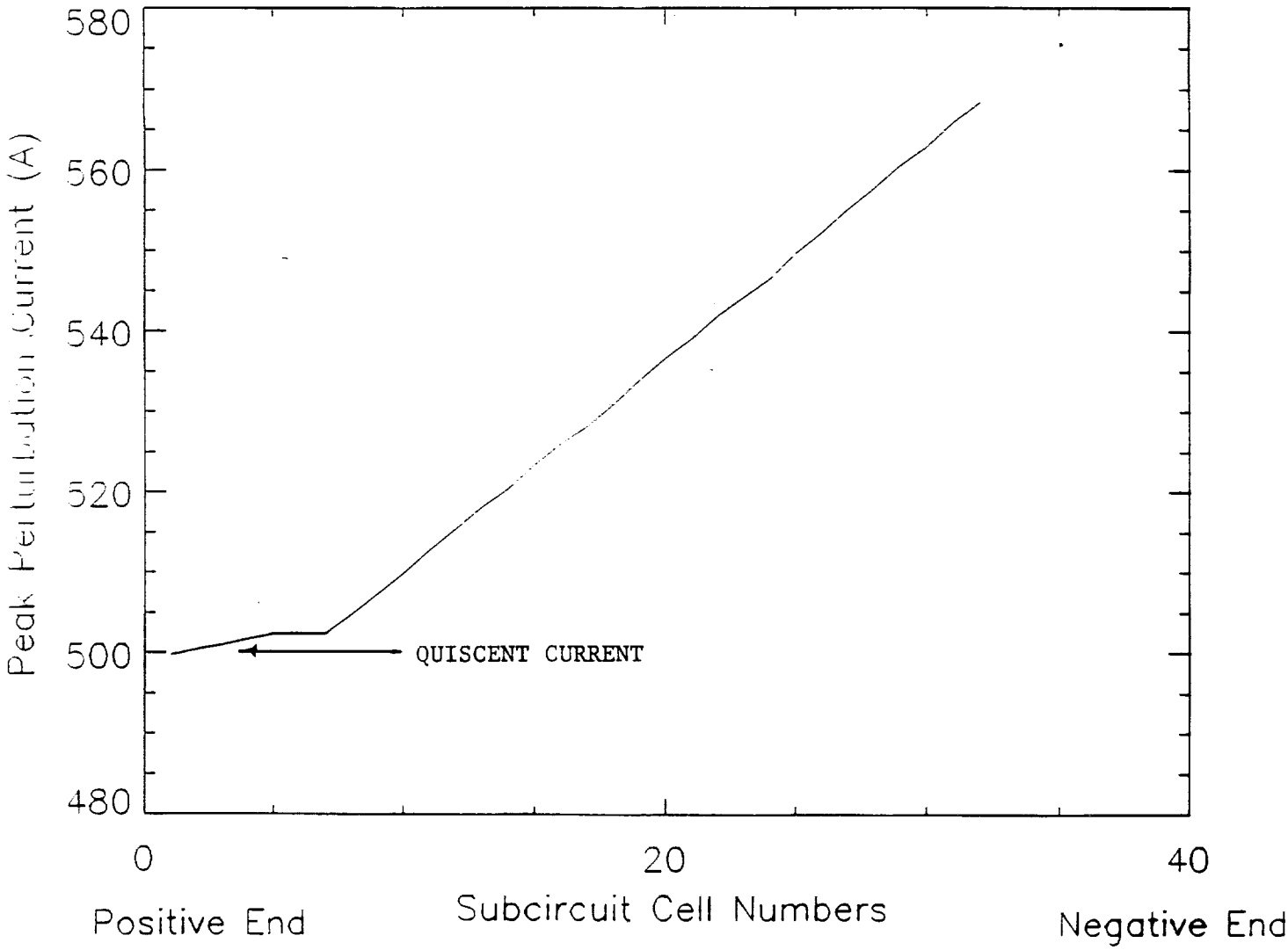

Figure 13 Perturbations in the array current as a function of subcircuit (solar cell group) cell number. The positive and negative ends are marked. Note that the perturbation over the quiscent current increases toward the negative end.

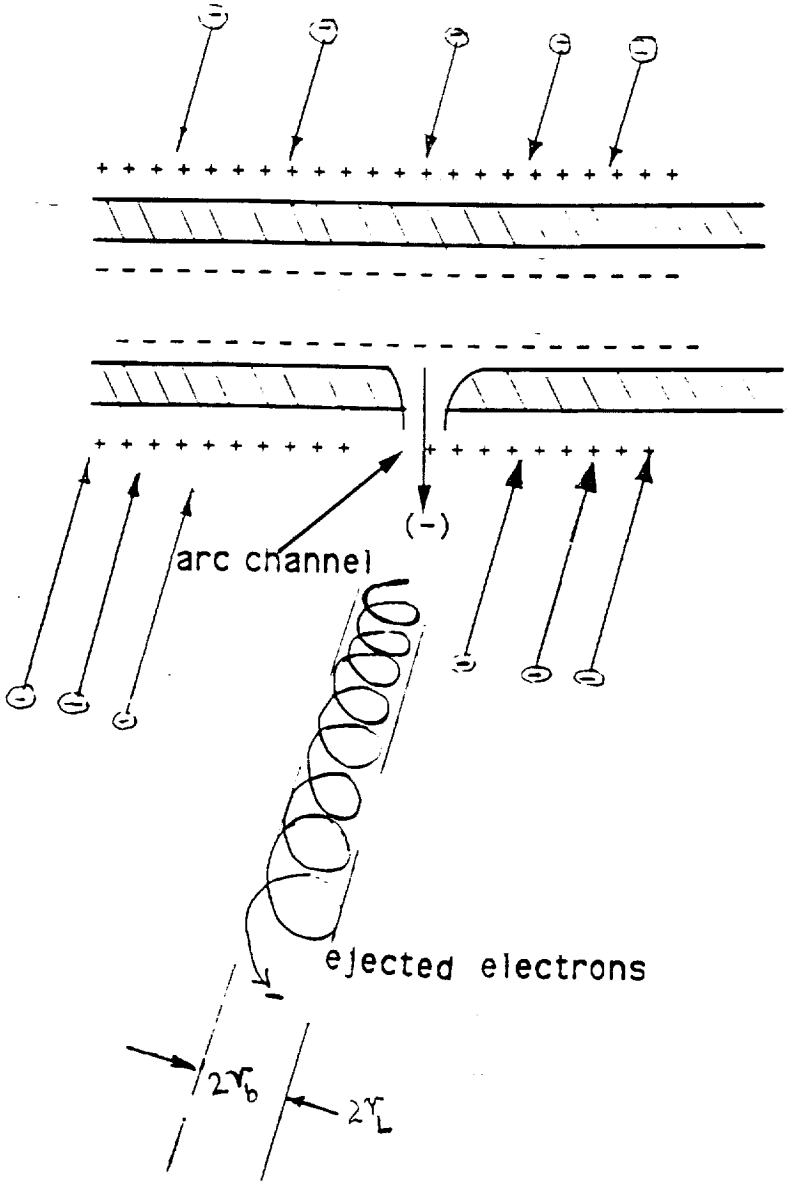

Figure 14

Schematic diagram indicating a possibility of how the electrons ejected during an arcing event escape into the ionospheric plasma along the earth's magnetic field. The left over positive charges near the structure are neutralized by a return electron current from the ambient plasma.

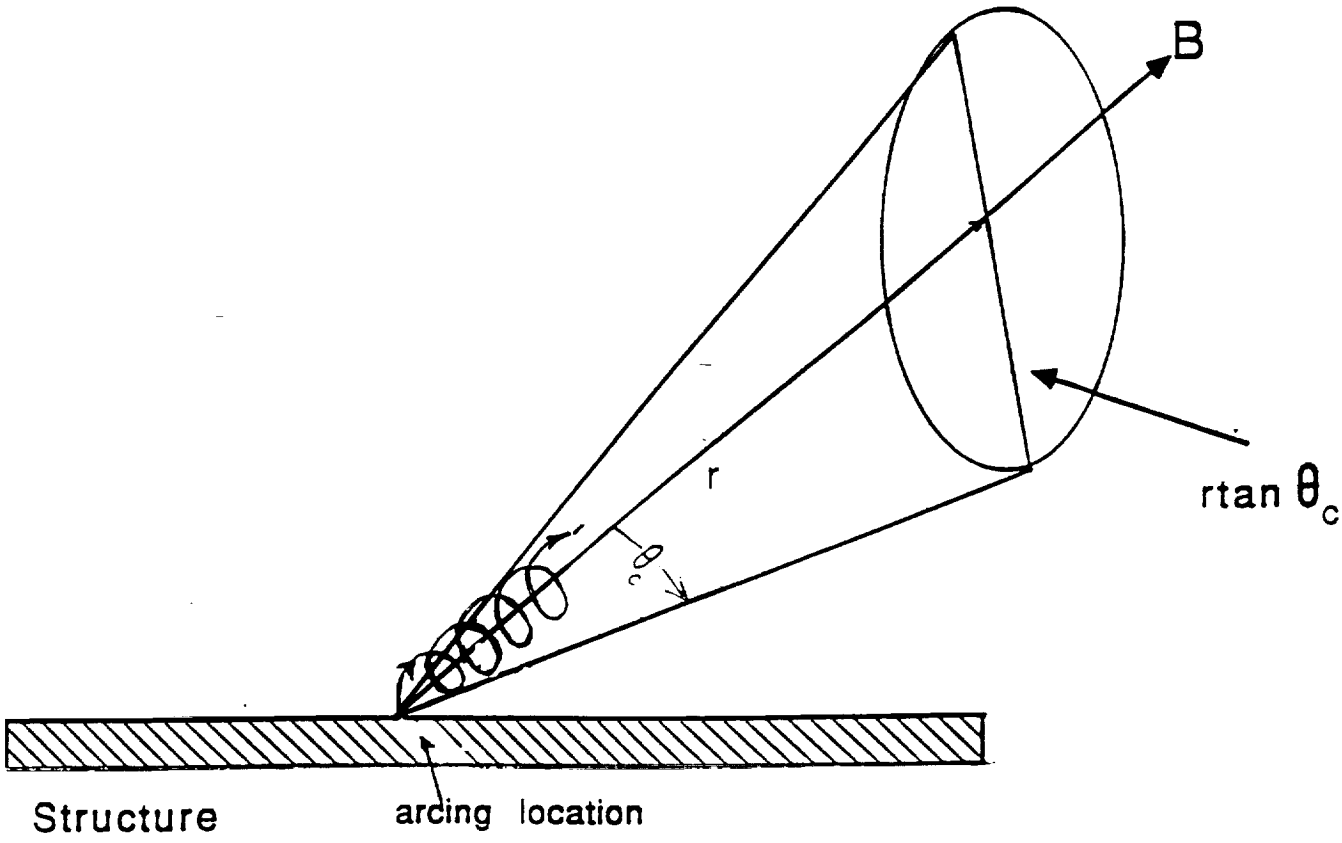

Figure 15

Cone of radiation of electromagnetic and plasma waves for $f_{lh} \leq f \leq f_{ce}$.

Report Documentation Page

1. Report No.	2. Government Accession No.	3. Recipient's Catalog No.
Final		

4. Title and Subtitle

STUDY OF PLASMA ENVIRONMENTS FOR THE INTEGRATED SPACE STATION ELECTROMAGNETIC ANALYSIS SYSTEM

5. Report Date

Aug. 26, 1992

6. Performing Organization Code

7. Author(s)

N. SINGH

8. Performing Organization Report No.

10. Work Unit No.

D. O. 133

9. Performing Organization Name and Address

UAH, Huntsville , Al 35899

11. Contract or Grant No.

NAS8-36955

13. Type of Report and Period Covered

monthly Final

12. Sponsoring Agency Name and Address

NASA/MSFC

14. Sponsoring Agency Code

15. Supplementary Notes

16. Abstract

The final report includes an analysis of various plasma effects on the electromagnetic environment of the Space Station Freedom. Effects of arcing are presented. Concerns of control of arcing by a plasma contactor are highlighted. Generation of waves by contaminant ions are studied and amplitude levels of the waves are estimated. Generation of electromagnetic waves by currents in the structure of the space station, driven by motional EMF, is analysed and the radiation level is estimated.

17. Key Words (Suggested by Author(s))	18. Distribution Statement
Arcing, Space Station Plasma, Waves, EM radiation.	

19. Security Class. (of this report)	20. Security Class. (of this page)	21. No. of pages	22. Price